Article

Cell Systems

Optimal Regulatory Circuit Topologies for Fold-Change Detection

Graphical Abstract

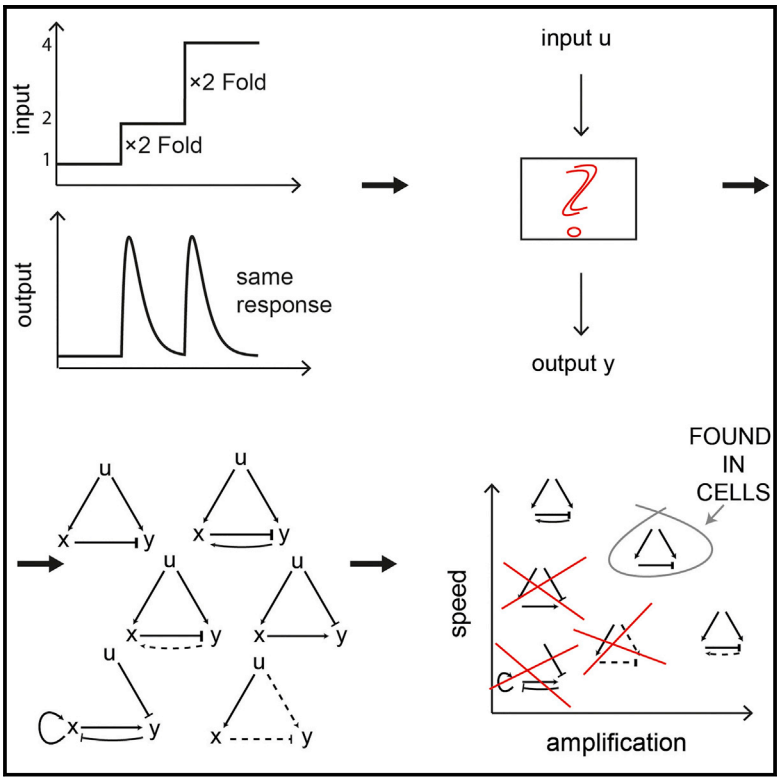

Highlights

- S-systems approach allows circuit screens that capture all parameters analytically
- We scanned ~500,000 circuits and found 644 fold-change detection circuits
- There are five minimal circuits that optimally trade off amplitude and speed
- The two experimentally observed circuits are among these five optimal circuits

Authors

Miri Adler, Pablo Szekely, Avi Mayo, Uri Alon

Correspondence

uri.alon@weizmann.ac.il

In Brief

Pareto optimality approach explains why evolution converges on only a few regulatory circuit designs that achieve fold-change detection.

Adler et al., 2017, Cell Systems *4*, 1–11
February 22, 2017
http://dx.doi.org/10.1016/j.cels.2016.12.009

CellPress

Please cite this article in press as: Adler et al., Optimal Regulatory Circuit Topologies for Fold-Change Detection, Cell Systems (2016), http://dx.doi.org/10.1016/j.cels.2016.12.009

Cell Systems
Article

Optimal Regulatory Circuit Topologies for Fold-Change Detection

Miri Adler,[1,2] Pablo Szekely,[1,2] Avi Mayo,[1] and Uri Alon[1,3,*]
[1]Department of Molecular Cell Biology, Weizmann Institute of Science, Rehovot 76100, Israel
[2]Co-first author
[3]Lead Contact
*Correspondence: uri.alon@weizmann.ac.il
http://dx.doi.org/10.1016/j.cels.2016.12.009

SUMMARY

Evolution repeatedly converges on only a few regulatory circuit designs that achieve a given function. This simplicity helps us understand biological networks. However, why so few circuits are rediscovered by evolution is unclear. We address this question for the case of fold-change detection (FCD): a response to relative changes of input rather than absolute changes. Two types of FCD circuits recur in biological systems—the incoherent feedforward and non-linear integral-feedback loops. We performed an analytical screen of all three-node circuits in a class comprising ~500,000 topologies. We find that FCD is rare, but still there are hundreds of FCD topologies. The two experimentally observed circuits are among the very few minimal circuits that optimally trade off speed, noise resistance, and response amplitude. This suggests a way to understand why evolution converges on only few topologies for a given function and provides FCD designs for synthetic construction and future discovery.

INTRODUCTION

Diverse regulatory systems in cells were recently found to respond to relative changes in input signal rather than to absolute changes (Lazova et al., 2011; Lee et al., 2014; Larsch et al., 2015). This feature is called fold-change detection (FCD). A system with FCD shows a dynamical output profile, including amplitude and response time, that is independent of multiplying the input by a constant. For example, a step in input signal from 1 to 2 results in exactly the same dynamical output profile as a step from 2 to 4 (Figure 1A), because both steps have the same fold change.

FCD combines two important features often found in sensory systems: Weber's law (Weber, 1905; Mesibov et al., 1973; Adler et al., 2014) and exact adaptation (Barkai and Leibler, 1997; Yi et al., 2000). Weber's law states that the response amplitude is proportional to the fold change in input. FCD implies Weber's law and in addition demands that the entire dynamical response profile, including response time, be a function only of fold change in input. All FCD systems also have exact adaptation, in which the steady-state output is independent on input level, but not all systems with exact adaptation have FCD, including the important example of linear integral feedback (Yi et al., 2000; El-Samad et al., 2002, 2005b).

The FCD property was defined experimentally and theoretically in the Wnt system (with Wnt signal as input and gene expression and embryo morphology as output; Goentoro and Kirschner, 2009; Goentoro et al., 2009) and in bacterial chemotaxis (input: chemoattractant; output: cheYp and tumbling frequency; Shoval et al., 2010; Lazova et al., 2011; Hamadeh et al., 2013). FCD was recently found experimentally in another signaling pathway, NFκB (input: NFκB level; output: gene expression; Lee et al., 2014). The dynamics of *dictyostelium* chemotaxis signaling measured by Takeda et al. (2012) shows hallmarks of FCD in response to extracellular cyclic AMP (cAMP) steps, as was discussed by theoretical analyses (Skataric and Sontag, 2012a; Adler et al., 2014). Sensory neurons in *C. elegans* were found to show FCD in response to odorants (Larsch et al., 2015). FCD is likely to occur also in *drosophila* wing development (Wartlick et al., 2011; Hironaka and Morishita, 2014) and has been suggested theoretically to appear in immunology (Sontag, 2015), cell growth (Furusawa and Kaneko, 2012), and in simple protein circuits (Buijsman and Sheinman, 2014; Olsman and Goentoro, 2016). FCD circuits have also been constructed synthetically (Kim et al., 2014; Table 1).

It is not easy for a circuit to achieve FCD, because the ability to detect fold change places constraints on the dynamics of the entire response. Theoretical work provided general conditions required for FCD (Shoval et al., 2010) and focused in detail on two main circuit designs: the incoherent type-1 feedforward loop (I1FFL) (Goentoro et al., 2009) and the non-linear integral feedback loop (NLIFL) (Tu et al., 2008; Shoval et al., 2010; Figures 1B and 1C). In both circuits, an internal variable x rises with the input signal but inhibits the output y in a way that normalizes out the input steady-state level.

FCD circuits were further studied theoretically. Hart et al. (2013) showed that the response of FCD circuits to multiple simultaneous signals is determined by the product of their fold changes. Marquez-Lago and Leier (2011) analyzed the stochastic behavior of FCD circuits. Shoval et al. (2011) generalized the FCD property, which is an invariance of the output to multiplying the input by a scalar (hence FCD is sometimes called scale invariance), to other forms of invariance. For example, recent work on endocrine circuits identified a class of circuits that shows invariance to certain physiological parameters, a feature called dynamic compensation (Karin et al., 2016).

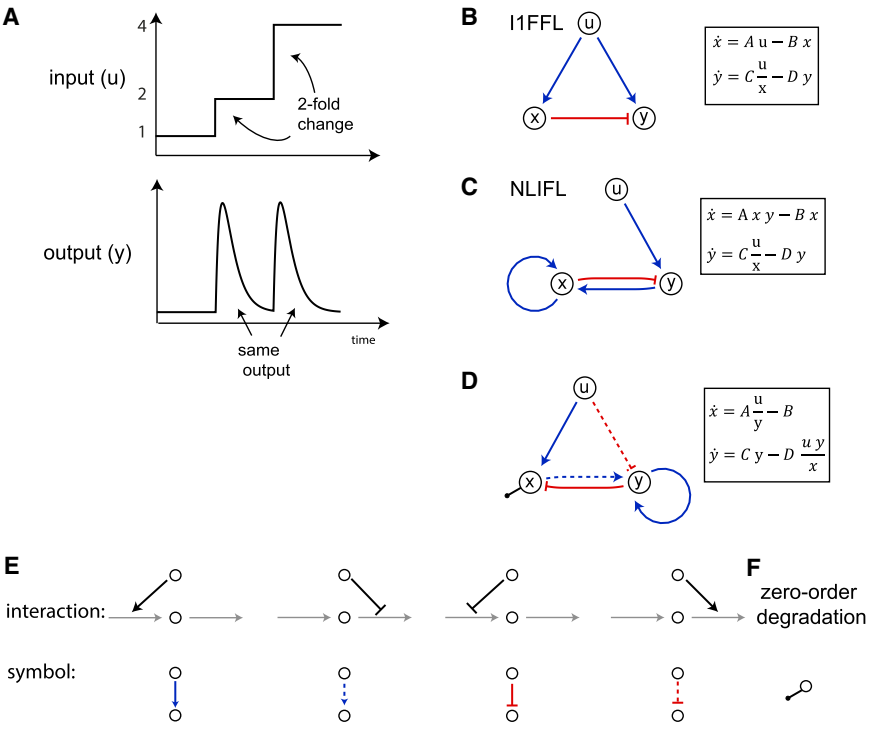

Figure 1. Search for Fold-Change Detection Circuits

(A) Fold-change detection provides an output profile that depends only on the fold change in the input.

(B and C) The two known naturally occurring FCD circuits are the type 1 incoherent feedforward loop (I1FFL) (B) and the non-linear integral feedback loop (NLIFL) (C). NLIFL occurs in bacterial chemotaxis, where the autoregulation is due to the exponential dependence on receptor methylation of the receptor affinity to ligand, as described in Tu et al. (2008) and Shoval et al. (2010).

(D) A non-FCD circuit included in the class we screen.

(E) Notation for the interactions included in the screen. Activation and inhibition are in blue and red, and effects on production and degradation rates are solid and dashed arrows, respectively.

(F) Symbol that represents zero-order degradation.

Experimentally, only two FCD circuit designs have been found so far (Table 1). The NLIFL (Figure 1C) is found in bacterial chemotaxis, and the I1FFL (Figure 1B) is found in all other systems. Here, we ask whether there are additional possible FCD regulatory circuits, and if so, how many? If there are many possible circuits, can we provide a rationale for why only two have been observed in the different biological systems studied so far? Do the two observed circuits have some functional advantage over the other possible FCD designs?

To address these questions, we develop a framework to analytically scan a wide class of circuits for the FCD property. We build on previous work that searched for features, such as robust morphogen patterning (Eldar et al., 2002, 2004), exact adaptation (Ma et al., 2009), ultrasensitivity (Shah and Sarkar, 2011), bistability (Yao et al., 2011), and cell polarization (Chau et al., 2012; Wang et al., 2013). Of special relevance is a screen for approximate FCD in a model of three enzymes by Skataric and Sontag (2012b), which defined a general principle for FCD based on separation of timescales between components. These screens faced the challenge of scanning many values for the biochemical parameters in each topology (topology is defined by the interactions in the circuit, and parameters describe the strength of each interaction). Therefore, these screens were usually limited to $\sim 10^4$ topologies.

To bypass the need for exhaustive parameter scans of each topology, we developed an analytically tractable class of regulatory circuits that allows us to solve for all values of parameters at once. This allowed us to screen a class of half a million circuit topologies. We find that the FCD property is very rare (0.1% of circuits), but we still discover hundreds of different circuit topologies that provide exact FCD. We then ask what is special about the two experimentally observed FCD topologies. We hypothesize that the observed circuits show optimal tradeoff between key tasks. To test this, we use a Pareto optimality approach (El Samad et al., 2005a; Shoval et al., 2012; Warmflash et al., 2012; Szekely et al., 2013; Boada et al., 2016). We demonstrate that the two topologies observed in biological systems are among the very few that show an optimal tradeoff of amplitude versus speed and amplitude versus noise resistance.

RESULTS

Screen of a Wide Class of Three-Node Circuits for Stability, Adaptation, and FCD

We consider a class of circuit models that covers a large number of topologies and is yet analytically tractable. The circuits have three nodes: input u; internal node x; and output y. The dynamics of x and y is governed by differential equations:

$$\frac{dx}{dt} = f(u,x,y); \quad (1)$$

$$\frac{dy}{dt} = g(u,x,y). \quad (2)$$

We employ biochemically reasonable forms for the functions f and g. Both functions are described as the difference between a production term and a removal term. These terms are often modeled by Michaelis-Menten-like terms (e.g., $x/(x+K_d)$ for activation; $K_d/(x+K_d)$ for inhibition). To capture the activation and inhibition forms in a way that is tractable, we use a simplified S-systems approach (Savageau, 1988): each term is a product of x, y, and u to the power of 0, 1, or -1. A zero power indicates no interaction; a +1 and -1 power indicate activation and inhibition, respectively. The S-systems form can be considered as the product of Michaelis-Menten-like terms in which the variable is much larger than K_d. This range $(x \gg K_d)$ is the relevant range

Table 1. Examples of Biological Systems that Show FCD or Have Been Suggested to Show FCD

System	Circuit	u	X	Y	Timescale of X/ Timescale of Y	Evidence	Ref.
Chemotaxis, *E. coli*	NLIFL	chemoattractant	receptor methylation	CheY-P (protein) tumbling rate	>1	experiment	Lazova et al., 2011
NF-κb, HeLa cells	I1FFL	NF-κb (transcription factor)	competitor (plausible candidate: p50/p52 homodimers)	inducible gene (e.g., IL8)	~1	experiment	Lee et al., 2014
Chemotaxis, *Dictyostelium discoideum*	I1FFL	cAMP (chemoattractant)	Ras-GAP (protein)	Ras-GTP (protein)	~1	experiment	Takeda et al., 2012
Chemotaxis, *C. elegans*	?	odorant	AIA (neuron)	AWA (neuron)	~1	experiment	Larsch et al., 2015
Synthetic in vitro system	I1FFL	DNA activator	iMG (RNA)	rMG (RNA)	>1	synthetic	Kim et al., 2014
Cell growth	?	nutrient	series of reactions	nutrient uptake	~1	theory	Furusawa and Kaneko, 2012
Drosophila wing development	I1FFL with NLIFL	DPP morphogen	regulatory circuit	cell number	~1	theory	Hironaka and Morishita, 2014
Immune systems	I1FFL	antigen	Treg (cells)	effector T cells (cells)	~1	theory	Sontag, 2015

for the two main known FCD mechanisms, I1FFL (Goentoro et al., 2009) and NLIFL (Tu et al., 2008; Shoval et al., 2010).

We presently do not consider cooperativity, which would involve powers larger than 1 or smaller than −1. Perhaps the main limitation of S-systems (with any powers) is that they do not allow multiple steady states, which can occur in certain biochemical systems. Known FCD circuits do not require cooperativity and do not have multiple steady states; expanding this study to include cooperativity and multiple steady states may uncover additional FCD possibilities.

Thus, our class of circuits is defined by

$$f(x,u,y) = Au^{\beta_{ux}}x^{\beta_{xx}}y^{\beta_{yx}} - Bu^{\alpha_{ux}}x^{\alpha_{xx}}y^{\alpha_{yx}}, \quad (3)$$

$$g(x,u,y) = Cu^{\beta_{uy}}x^{\beta_{xy}}y^{\beta_{yy}} - Du^{\alpha_{uy}}x^{\alpha_{xy}}y^{\alpha_{yy}}, \quad (4)$$

where $\alpha_{ij}, \beta_{ij} \in \{-1, 0, 1\}$ and A, B, C, and D are parameters.

Three examples of circuits in this class are shown in Figure 1, including the commonly observed I1FFL (Figure 1B) and the bacterial chemotaxis NLIFL circuit (Figure 1C).

To simplify the analysis, we transform to dimensionless equations by rescaling the equations to have only one dimensionless parameter group, T, equal to the ratio of the typical timescale of x and y (see STAR Methods). Hereafter, we use the dimensionless equations:

$$\frac{dx}{dt} = u^{\beta_{ux}}x^{\beta_{xx}}y^{\beta_{yx}} - u^{\alpha_{ux}}x^{\alpha_{xx}}y^{\alpha_{yx}}; \quad (5)$$

$$T^{-1}\frac{dy}{dt} = u^{\beta_{uy}}x^{\beta_{xy}}y^{\beta_{yy}} - u^{\alpha_{uy}}x^{\alpha_{xy}}y^{\alpha_{yy}}. \quad (6)$$

Because there are 12 power parameters $(\alpha_{ij}, \beta_{ij})$, which can each take on one of three values, there are overall $3^{12} \sim 5\times10^5$ circuits.

We use a graphical notation system to denote these circuit topologies (Figure 1E). Each circuit is represented by a graph with solid lines for interaction in production terms and dashed lines for interactions in the removal terms.

We further identify subclasses of circuits with special biological meaning. Circuits in which the removal rate of a variable is linear in the variable, as occurs for most non-saturated biochemical removal processes, such as dilution and active degradation, are called natural circuits (examples are in Figures 1B and 1C, but not Figure 1D, which has a zero-order removal of x). There are $\sim 5.9\times10^4$ natural circuit topologies. An important subclass of the natural circuits allows only interactions between variables in the production terms, but not the removal terms, as occurs in purely transcription circuits. We call this the transcriptional circuit subclass, which includes 729 topologies (see STAR Methods).

We next screened the circuits for features of interest, focusing on the 99% of the circuits that have a connected topology diagram. We tested whether a steady state exists. For this purpose, we solved $f(u,x,y) = g(u,x,y) = 0$ and analytically sought non-zero solutions (recall that, in the present class, there is at most one non-zero steady state). Sixty-four percent of the circuits had a non-zero steady state (see STAR Methods).

Next, we determined the stability of the steady state by analytically computing the Jacobian (see STAR Methods). We find that

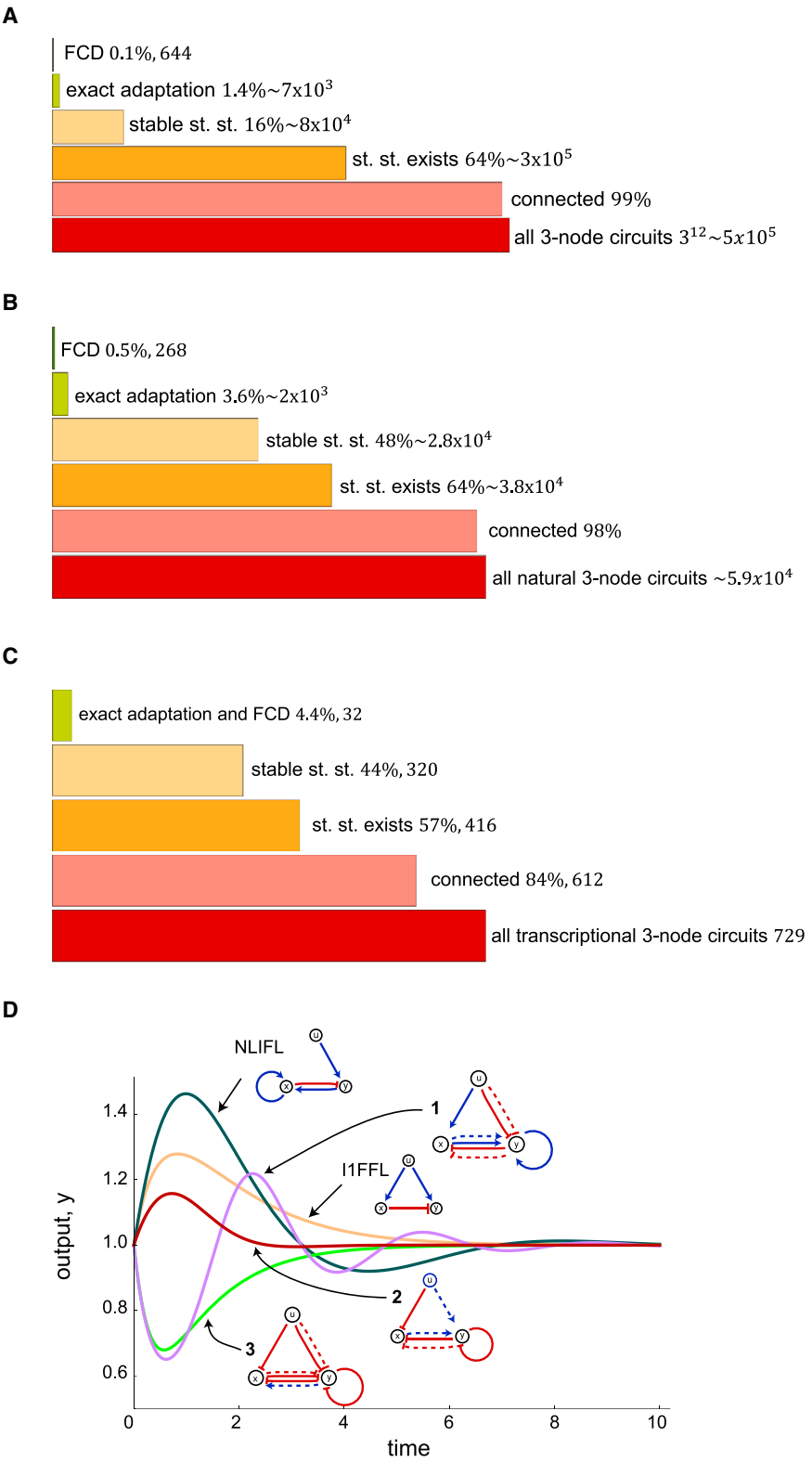

Figure 2. There Are Many FCD Circuits, but They Are Rare among the Entire Space of Possible Topologies

(A–C) Bar plots for various circuit properties. (A) All circuits screened, (B) subclass of circuits with linear degradation (natural circuits), and (C) subclass of natural circuits with interactions only on production rates (transcription circuits) are shown.

(D) The dynamics of the response to a step in u (from 1 to 2) of the two observed circuits, I1FFL and NLIFL, are plotted as well as dynamics of other FCD circuits found in the screen: oscillatory response (1); small amplitude (2); and inverse output response (3). T = 1 throughout.

16% of the circuits have a stable steady state at least for some values of the dimensionless timescale ratio T. Most of these (88%) have a stable steady state for all values of T.

We next asked which stable circuits exhibit exact (or perfect) adaptation, which is a pre-requisite for FCD (Shoval et al., 2010). Exact adaptation is defined by a y steady state that is independent of u (see STAR Methods). This property turns out to be independent of T. We find that 1.4% of all circuits have exact adaptation of y in response to step changes in u. Thus, circuits with exact adaptation are relatively common, making up about 9% of the circuits with a stable steady state. Figure 2 summarizes these properties.

FCD Circuits Are Very Rare but Still There Are Hundreds of FCD Designs

We next performed a screen for the FCD property. For this purpose, we note that the homogeneity conditions of Shoval et al. (2010), which are sufficient conditions for FCD in general, turn out to also be necessary for FCD in the present class of circuits (for proof, see STAR Methods). Therefore, we can use the homogeneity conditions to discover all FCD circuits in the class (see STAR Methods).

We find that the FCD property is very rare: only 0.1% of all circuits (644) have the FCD property. All FCD circuits have exact adaptation, but only 8.7% of the circuits with exact adaptation have FCD.

FCD circuits make up 0.5% of natural circuits (268) and 4.4% of transcriptional circuits (32; in the transcriptional subclass, all circuits with exact adaptation also have FCD). Although rare, there are 268 distinct natural FCD circuits.

The FCD circuits found here show a symmetry where each circuit with $x \sim u$ has a counterpart with $x \sim 1/u$, which can be derived by transforming $u \rightarrow 1/u$. From now on, we will consider only half of the circuits, with $x \sim u$.

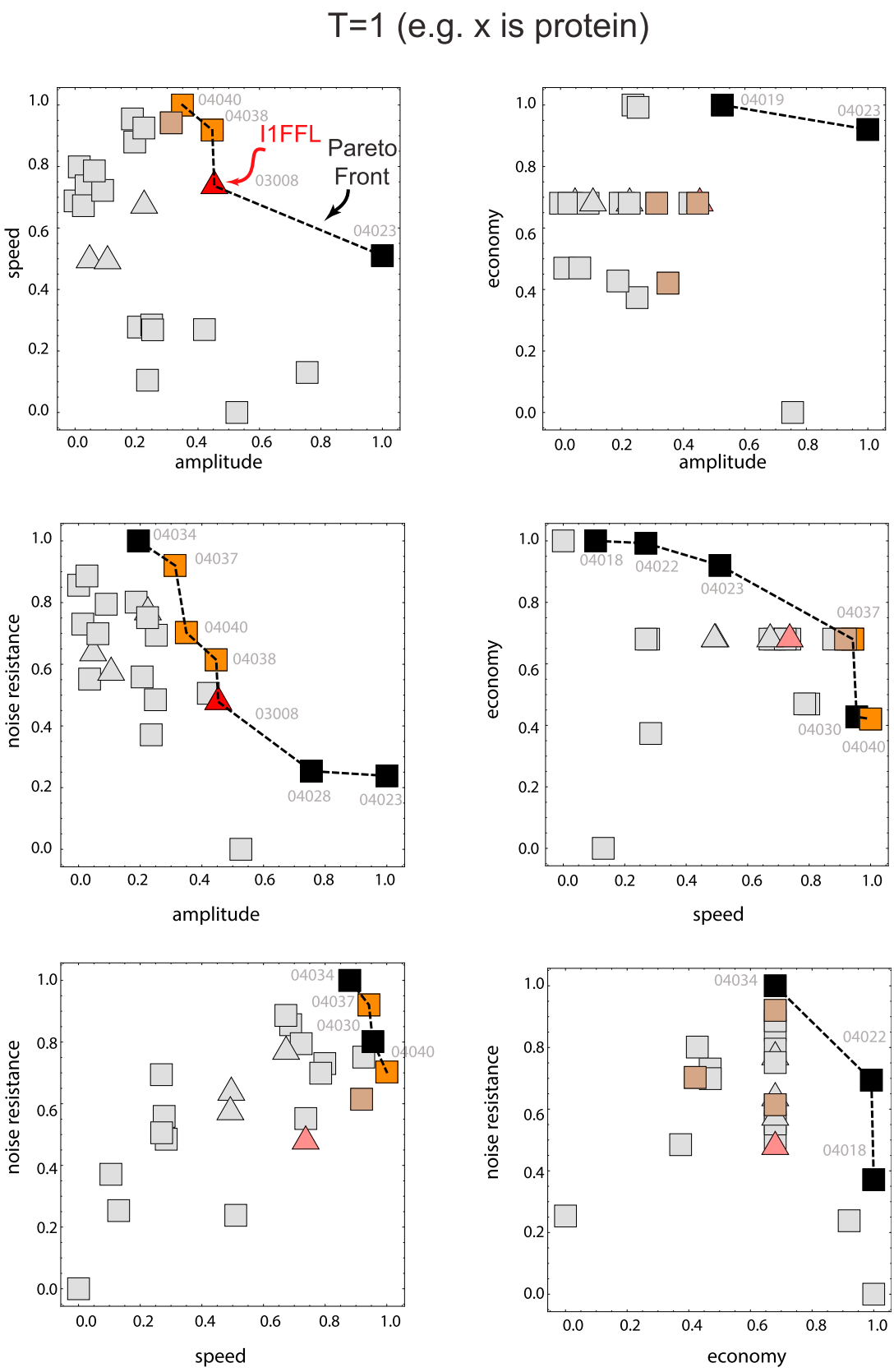

(legend on next page)

FCD Circuits Can Show Diverse Response Dynamics

The different FCD circuits show various types of dynamics. Eighty-one percent have imaginary eigenvalues for some values of T and hence can show damped oscillations (Figure 2D, circuit 1). FCD circuits that are purely feedforward (no feedback in their graphs), such as the I1FFL, have strictly real eigenvalues and hence never show oscillations (Figure 2D).

Half of the FCD circuits show an inverse response in which y decreases when u increases (Figure 2D, circuit 3). The FCD circuits also differ in their amplitude and response time to a given step change in input u. The response amplitude to a 2-fold input step, with $T = 1$, varies between FCD topologies by a factor of 7, and response time varies by a factor of 4.

The Observed FCD Circuits Are Pareto Optimal for Speed, Amplitude, and Noise Resistance

We finally asked whether one can classify the FCD circuits based on their dynamic features. We considered four dynamical tasks that are thought to be important for biological circuits (El Samad et al., 2005a; Savageau, 2001; Szekely et al., 2013): speed; amplitude; economy (defined using the production rate of the internal node x); and noise resistance (deviation from steady-state given noise in the dynamical equations).

We further considered that evolutionary processes often result in circuits with the smallest number of interactions (Burda et al., 2010; Friedlander et al., 2013, 2015), because mutations more often remove an interaction than build a new one. Moreover, interaction arrows in a circuit typically carry a fitness cost (e.g., cost of producing, maintaining, and cross-talk of transcription factors; Dekel and Alon, 2005; Itzkovitz et al., 2006; Clune et al., 2013; Kafri et al., 2016; Friedlander et al., 2016). We therefore compare circuits with the smallest number of interactions, four or less, resulting in 24 natural circuits.

Because the four tasks we consider depend strongly on the timescales of the system T, we consider separately two distinct biological cases: (1) the first is circuits in which x and y have a similar timescale. This occurs in IFFLs in which x is a transcription factor and y is an output protein, for example, in the NFκB system, or when x and y are both signaling proteins, as in *dictyostelium* chemotaxis. (2) The second is circuits in which x is much slower than y. This occurs in bacterial chemotaxis where x is a receptor methylation that changes over minutes and y represents phosphorylation of CheY that changes over seconds. We represent these cases by two typical values for T, the dimensionless ratio of the timescales of x and y: $T = 1$ and $T = 10$ (see STAR Methods for $T = 0.1$).

For these two timescale cases, we plotted how the circuits do in all six pairs of the four tasks in response to large input steps. We define the tasks as follows: response amplitude is the maximal deviation of output from steady state: $a = \max|y(t) - y_{st}|$. Speed is the inverse of the response time, $s = t_{res}^{-1}$, where the response time is defined by the center of mass of the response curve $t_{res} = \int t|y(t) - y_{st}|\,dt / \int|y(t) - y_{st}|\,dt$. Economy is defined by the production rate of x, $P = u^{\beta_{ux}} x^{\beta_{xx}} y^{\beta_{yx}}$, integrated over the response $e = -\int_0^\infty (P - P_{steady\ state})dt$. Noise resistance is one over the numerically computed SD of the output y around its steady state when multiplicative white noise is introduced to x and y (STAR Methods). Each circuit is represented by a point in these two-task plots (Figures 3, 4, and S1).

We find that there is a general tradeoff between several of the tasks, such as amplitude and response time, as seen by the negative overall slope of some of the scatterplots. To seek the circuits that are the best multi-taskers, we used the Pareto front approach (Szekely et al., 2013; Boada et al., 2016). For every pair of tasks, we removed each circuit Q, which is dominated by another circuit W, in the sense that W is better at both tasks than Q. After removing all dominated circuits, we remain with the Pareto front. The Pareto front is the set of all circuits that cannot be improved simultaneously in both tasks.

We find that the experimentally observed circuits—I1FFL and NLIFL—lie on the Pareto front of their respective timescale class in terms of speed and amplitude (red triangle/square in Figures 3 and 4) and in terms of noise resistance and amplitude. The observed circuits lie quite close to the front for most of the other pairs of tasks.

We consider the Pareto front for speed and amplitude in more detail (Figures 5 and S2). The two observed circuits are among the five circuits that lie on the front. The other three circuit topologies on the Pareto fronts are interesting possible mechanisms for future discovery. Their topology and dynamics are shown in Figure 5 (see Figure S3 for T = 0.1).

For T = 1, the I1FFL, which occurs in large numbers in gene-regulation networks (Alon, 2006), is the only feedforward circuit on the front. The front has a kink in which adding one interaction to the I1FFL results in an improvement in speed at similar amplitude (circuit 04038 in Figure 5A). Other forms of incoherent feedforward loops, such as the type-3 IFFL (I3FFL), are off the front. This functional advantage may contribute to the prevalence of I1FFL compared to other incoherent feedforward topologies in gene-regulation networks (Mangan and Alon, 2003; Mangan et al., 2006).

For T = 10, the observed NLIFL circuit (found in bacterial chemotaxis) is one of three possible feedback designs on the front. These topologies have similar interaction signs in which x inhibits y and y activates x but differ by the mode of activation

Figure 3. The Experimentally Observed I1FFL Circuit Is on the Pareto Front for Amplitude versus Speed and Noise Resistance for T = 1

All natural FCD circuits with three interactions (triangles) or four interactions (squares) are plotted according to all pairs of four tasks: speed; amplitude; noise resistance; and economy, for T = 1. The tasks are computed for a large step in input (100-fold). In each plot, the black points and dashed line are the Pareto front, defined as the set of circuits that are not dominated on both tasks by any other circuit. The experimentally observed circuit (I1FFL with T = 1) is indicated in red when on the front and pink when off the front. Circuits on the Pareto front are numbered and listed in Table S1. Circuits that are one interaction away from the I1FFL are denoted in orange if they are on the front and brown if they are off the front (see Figure S1 for the same figure only for T = 0.1). The axes for speed, amplitude, and noise resistance are the log-transformed value of the performance in each task, rescaled (after log transform) between zero and one. Economy e can have zero or negative values for some circuits because it is defined relative to the production rate in the post-step steady state. Hence, to avoid divergence, the economy axis is defined by $log(1 + |e|)sgn(e)$, rescaled between zero and one, where $sgn(e)$ is 1 when $e > 0$ and −1 when $e < 0$.

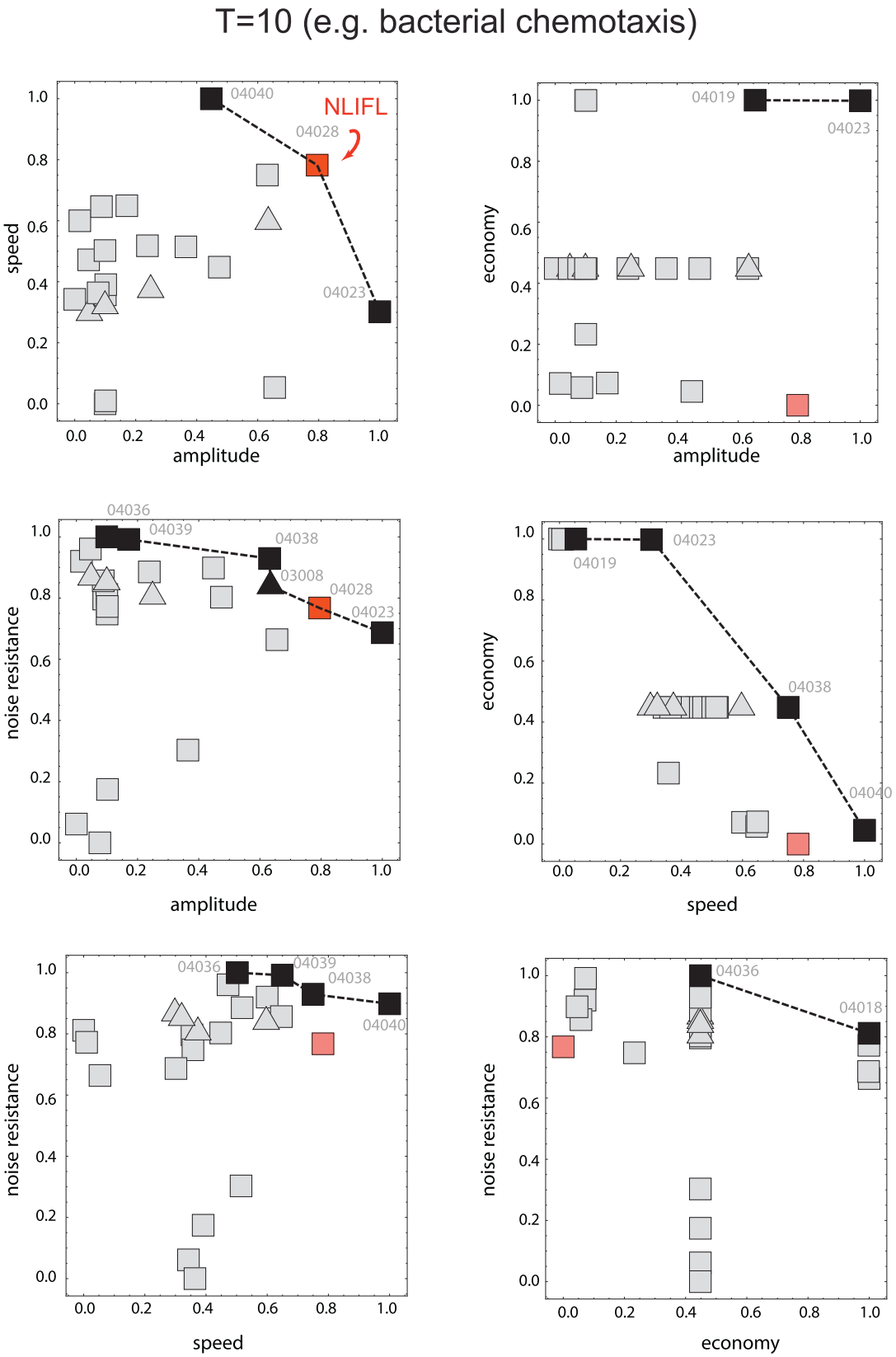

Figure 4. The Experimentally Observed NLIFL Circuit Is on the Pareto Front for Amplitude versus Speed and Noise Resistance for T = 10
This figure is the same as Figure 4, except that T = 10, and the observed circuit is the NLIFL.

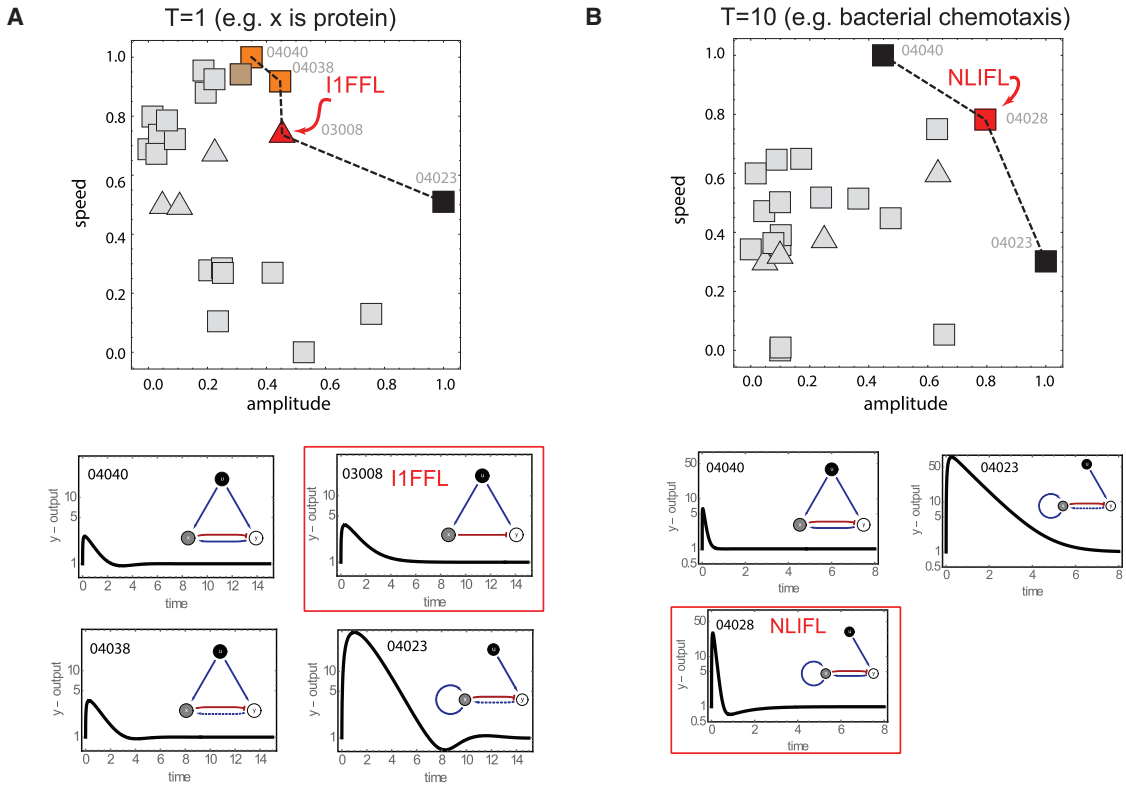

Figure 5. The Speed-Amplitude Pareto Front Suggests Several FCD Circuits with Optimal Tradeoff

Circuits topologies on the front and their dynamics in response to a large input step (100-fold) for (A) T = 1 and (B) T = 10 (see the topology and dynamics of circuits that lie close to the Pareto front for T = 1 in Figure S2, S3 for a similar figure only with T = 0.1, and Figure S4 for a version of this figure with a smaller input step, 2-fold).

(production or removal) and the presence/absence of x autoregulation. The $T = 10$ circuits on the front are overall much faster than the $T = 1$ circuits. One may hypothesize that, for speed, a large separation of timescales between x and y is useful.

Up to now, we considered topologies with at most four interaction arrows. Adding topologies with five arrows changes the fronts (Figure 6; tables of all circuits and their performances at the tasks are provided in Table S1). The bacterial chemotaxis circuit (NLIFL with $T = 10$) remains on the speed-amplitude front, outperforming five-interaction circuits (Figure 6B). The I1FFL with $T = 1$ drops slightly below the speed-amplitude front. The front does include, however, two circuits that are one edge away from the I1FFL (orange markers), which may be candidates for future discovery (circuits 04040 and 04038 in Figure 6A). We conclude that selection for minimal number of interactions and for the tradeoff between speed, noise resistance, and amplitude may be good candidates for the evolutionary forces that lead to the experimentally observed FCD topologies.

DISCUSSION

We scanned a wide class of three-node regulatory circuits for the exact fold-change detection property. Using dimensional analysis, we could scan the full class of 3^{12} circuits for all possible parameters analytically. We find that FCD is very rare, amounting to 0.1% of circuits. The FCD property appears to be much rarer than the exact adaptation property (1.4% of circuits). Although rare, due to the large number of possible circuits, we discovered hundreds of different circuit topologies that can provide FCD.

We compared all natural minimal topologies in terms of four key tasks (Savageau, 1976; Savageau, 2001; Szekely et al., 2013): amplitude; response time; noise resistance; and economy. We find that the two observed FCD circuits lie on the Pareto fronts for speed versus amplitude and for noise resistance versus amplitude. In other words, no other circuit with comparable number of interactions dominates the observed circuits in both speed and amplitude or noise resistance and amplitude. Speed, amplitude, and noise resistance are plausible as important tasks for the natural selection of such circuits. It is often desirable to have large response amplitude in order to overcome molecular noise and provide a suitable biological output; rapid responses are advantageous in order to track rapidly changing chemotaxis gradients or to produce output proteins in time to respond to external signals (Camas et al., 2006; Mangan et al., 2006; Rosenfeld et al., 2002; Savageau, 2001), and noise resistance is thought to be an important task due to prevalent molecular noise in biological circuits (Elowitz et al., 2002; Paulsson, 2004; Raser and O'Shea, 2005; Bar-Even et al., 2006; Sigal et al., 2006).

We suggest more generally that the limited number of topologies that optimally trade off important design features is one explanation for why very few topologies actually appear in

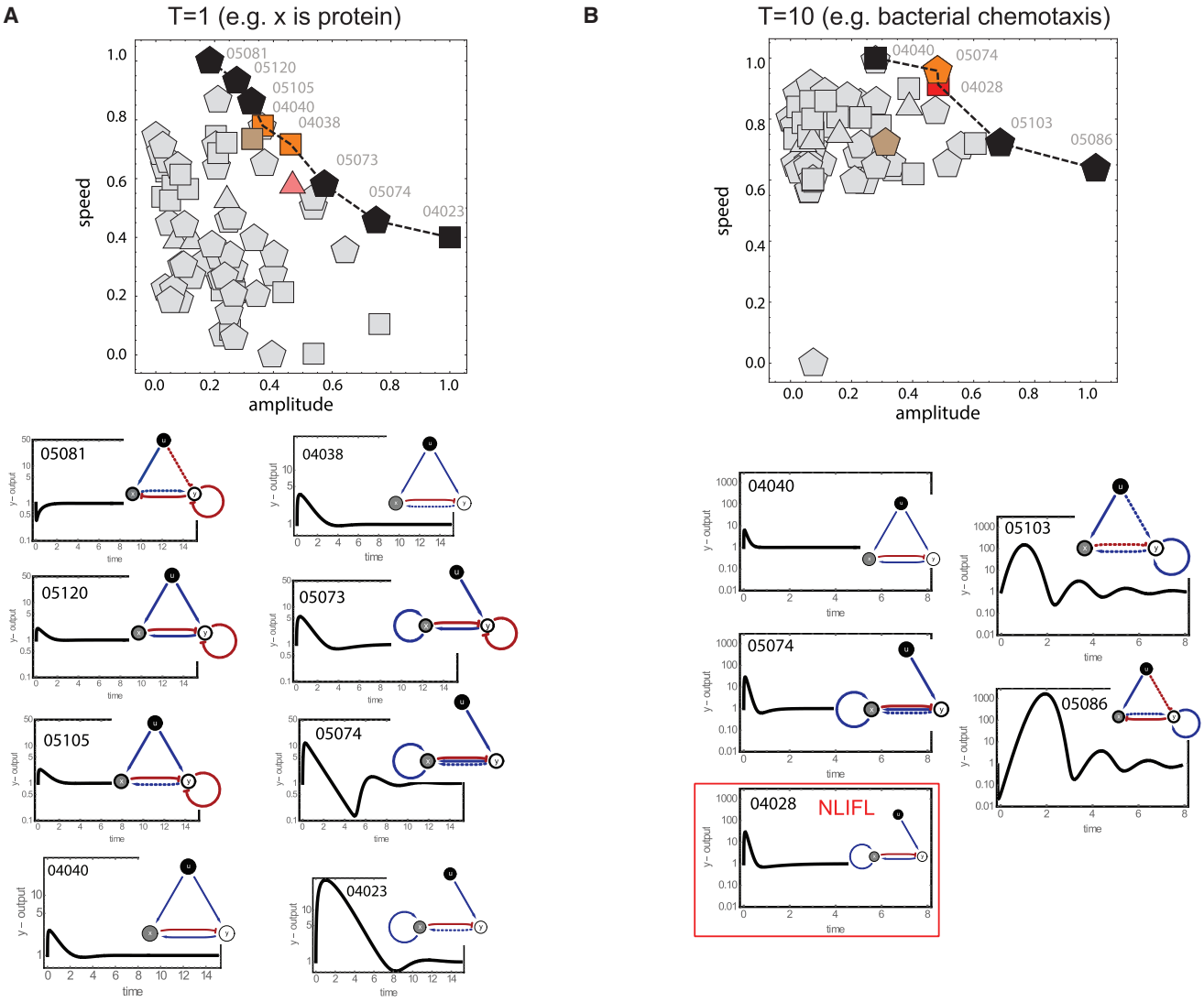

Figure 6. Adding Circuits with Five Interactions Moves the Pareto Front, but the Observed Circuits Remain on the Front or Close to the Front
Circuits with five interactions (pentagons) are shown together with circuits with three (triangle) or four (square) interactions. The observed circuits are in bright red (on the front) or pink (off the front). Topology and dynamics of the circuits on the front are shown in response to a large step (100-fold).

biological systems (Alon, 2007; Milo et al., 2002). An alternative possibility is experimental bias, in which the known topologies are those that are actively tested and thus more likely to be discovered. Our analysis presents several new FCD circuits that are Pareto optimal and have not yet been discovered experimentally. It would be of interest to see whether these are found in biology or whether they have some disadvantage that precludes their use.

Previous use of the Pareto approach for biological circuits compared a few topologies (Warmflash et al., 2012) for the sign-sensitive delay property or compared different parameter values for a single topology of a stress-response feedback circuit (El Samad et al., 2005a; Szekely et al., 2013). The present use of Pareto optimality can in principle suggest which tasks may have been important for the selection of the circuits (speed, amplitude, and noise resistance in the present case). We note that Pareto optimality can also be used in a different way when the tasks are unknown à priori: the tasks at play can be discovered from the vertices of polygonal or polyhedral structures in data (Shoval et al., 2012; Korem et al., 2015; Szekely et al., 2015; Tendler et al., 2015)—an approach known as Pareto task inference (Hart et al., 2015).

The present use of a wide yet analytically tractable class—the simplified S-systems—allows scanning of large numbers of topologies for all possible parameters, without need for exhaustive parameter sampling. Pareto optimal designs for desired biological functions can inform the synthetic biology design of new circuits. For the point of view of fundamental scientific understanding, this study aligns with the hope that important functions, such as FCD, will be carried out across organisms by only a small set of possible circuits, increasing the comprehensibility of biological systems (Alon, 2003).

STAR★METHODS

Detailed methods are provided in the online version of this paper and include the following:

- KEY RESOURCES TABLE
- CONTACT FOR REAGENT AND RESOURCE SHARING
- METHOD DETAILS
  - Dimensional analysis of the S-systems dynamical equations
  - Definition of natural and transcriptional circuit subclasses
  - Analytical screen of circuit properties
  - Analytical solution for the Jacobian
  - Proof that the homogeneity conditions from Shoval et al. are sufficient and necessary for FCD in the S-systems framework
  - The FCD circuits in our screen show a symmetry
  - Speed and amplitude calculation
  - Noise resistance calculation
  - FCD circuits in which the internal node x is faster than the output y (T = 0.1)

SUPPLEMENTAL INFORMATION

Supplemental Information includes four figures and one table and can be found with this article online at http://dx.doi.org/10.1016/j.cels.2016.12.009.

AUTHOR CONTRIBUTIONS

Conceptualization, M.A., P.S., A.M., and U.A.; Software, P.S.; Formal Analysis, M.A., P.S., and A.M.; Data Curation, M.A.; Writing – Original Draft, M.A., P.S., and U.A.; Corresponding Author and Supervision, U.A.

ACKNOWLEDGMENTS

We thank H. Sheftel, J. Hausser, A. Tendler, Y. Korem, and members of the U.A. lab for discussions. This work was supported by the Israel Science Foundation grant number 1349/15. U.A. is the incumbent of the Abisch-Frenkel Professorial Chair.

Received: June 2, 2016
Revised: September 21, 2016
Accepted: December 8, 2016
Published: January 11, 2017

REFERENCES

Adler, M., Mayo, A., and Alon, U. (2014). Logarithmic and power law input-output relations in sensory systems with fold-change detection. PLoS Comput. Biol. *10*, e1003781.

Alon, U. (2003). Biological networks: the tinkerer as an engineer. Science *301*, 1866–1867.

Alon, U. (2006). An Introduction to Systems Biology: Design Principles of Biological Circuits (Boca Raton, FL: Chapman and Hall/CRC).

Alon, U. (2007). Network motifs: theory and experimental approaches. Nat. Rev. Genet. *8*, 450–461.

Bar-Even, A., Paulsson, J., Maheshri, N., Carmi, M., O'Shea, E., Pilpel, Y., and Barkai, N. (2006). Noise in protein expression scales with natural protein abundance. Nat. Genet. *38*, 636–643.

Barkai, N., and Leibler, S. (1997). Robustness in simple biochemical networks. Nature *387*, 913–917.

Boada, Y., Reynoso-Meza, G., Picó, J., and Vignoni, A. (2016). Multi-objective optimization framework to obtain model-based guidelines for tuning biological synthetic devices: an adaptive network case. BMC Syst. Biol. *10*, 27.

Buijsman, W., and Sheinman, M. (2014). Efficient fold-change detection based on protein-protein interactions. Phys. Rev. E Stat. Nonlin. Soft Matter Phys. *89*, 022712.

Burda, Z., Krzywicki, A., Martin, O.C., and Zagorski, M. (2010). Distribution of essential interactions in model gene regulatory networks under mutation-selection balance. Phys. Rev. E Stat. Nonlin. Soft Matter Phys. *82*, 011908.

Camas, F.M., Blázquez, J., and Poyatos, J.F. (2006). Autogenous and nonautogenous control of response in a genetic network. Proc. Natl. Acad. Sci. USA *103*, 12718–12723.

Chau, A.H., Walter, J.M., Gerardin, J., Tang, C., and Lim, W.A. (2012). Designing synthetic regulatory networks capable of self-organizing cell polarization. Cell *151*, 320–332.

Clune, J., Mouret, J.-B., and Lipson, H. (2013). The evolutionary origins of modularity. Proc. Biol. Sci. *280*, 20122863.

Dekel, E., and Alon, U. (2005). Optimality and evolutionary tuning of the expression level of a protein. Nature *436*, 588–592.

Ebert, M.S., and Sharp, P.A. (2012). Roles for microRNAs in conferring robustness to biological processes. Cell *149*, 515–524.

El-Samad, H., Goff, J.P., and Khammash, M. (2002). Calcium homeostasis and parturient hypocalcemia: an integral feedback perspective. J. Theor. Biol. *214*, 17–29.

El Samad, H., Khammash, M., Homescu, C., and Petzold, L. (2005a). Optimal performance of the heat-shock gene regulatory network. IFAC Proc. *Volumes 38*, 19–24.

El-Samad, H., Kurata, H., Doyle, J.C., Gross, C.A., and Khammash, M. (2005b). Surviving heat shock: control strategies for robustness and performance. Proc. Natl. Acad. Sci. USA *102*, 2736–2741.

Eldar, A., Dorfman, R., Weiss, D., Ashe, H., Shilo, B.-Z., and Barkai, N. (2002). Robustness of the BMP morphogen gradient in Drosophila embryonic patterning. Nature *419*, 304–308.

Eldar, A., Shilo, B.-Z., and Barkai, N. (2004). Elucidating mechanisms underlying robustness of morphogen gradients. Curr. Opin. Genet. Dev. *14*, 435–439.

Elowitz, M.B., Levine, A.J., Siggia, E.D., and Swain, P.S. (2002). Stochastic gene expression in a single cell. Science *297*, 1183–1186.

Friedlander, T., Mayo, A.E., Tlusty, T., and Alon, U. (2013). Mutation rules and the evolution of sparseness and modularity in biological systems. PLoS ONE *8*, e70444.

Friedlander, T., Mayo, A.E., Tlusty, T., and Alon, U. (2015). Evolution of bow-tie architectures in biology. PLoS Comput. Biol. *11*, e1004055.

Friedlander, T., Prizak, R., Guet, C.C., Barton, N.H., and Tkačik, G. (2016). Intrinsic limits to gene regulation by global crosstalk. Nat. Commun. *7*, 12307.

Furusawa, C., and Kaneko, K. (2012). Adaptation to optimal cell growth through self-organized criticality. Phys. Rev. Lett. *108*, 208103.

Goentoro, L., and Kirschner, M.W. (2009). Evidence that fold-change, and not absolute level, of β-catenin dictates Wnt signaling. Mol. Cell *36*, 872–884.

Goentoro, L., Shoval, O., Kirschner, M.W., and Alon, U. (2009). The incoherent feedforward loop can provide fold-change detection in gene regulation. Mol. Cell *36*, 894–899.

Hamadeh, A., Ingalls, B., and Sontag, E. (2013). Transient dynamic phenotypes as criteria for model discrimination: fold-change detection in Rhodobacter sphaeroides chemotaxis. J. R. Soc. Interface *10*, 20120935.

Hart, Y., Mayo, A.E., Shoval, O., and Alon, U. (2013). Comparing apples and oranges: fold-change detection of multiple simultaneous inputs. PLoS ONE *8*, e57455.

Hart, Y., Sheftel, H., Hausser, J., Szekely, P., Ben-Moshe, N.B., Korem, Y., Tendler, A., Mayo, A.E., and Alon, U. (2015). Inferring biological tasks using Pareto analysis of high-dimensional data. Nat. Methods *12*, 233–235.

Hironaka, K., and Morishita, Y. (2014). Cellular sensory mechanisms for detecting specific fold-changes in extracellular cues. Biophys. J. *106*, 279–288.

Itzkovitz, S., Tlusty, T., and Alon, U. (2006). Coding limits on the number of transcription factors. BMC Genomics *7*, 239.

Kafri, M., Metzl-Raz, E., Jona, G., and Barkai, N. (2016). The cost of protein production. Cell Rep. *14*, 22–31.

Karin, O., Swisa, A., Glaser, B., Dor, Y., and Alon, U. (2016). Dynamical compensation in physiological circuits. Mol Sys Biol. *12*, 886.

Kim, Dh., Grün, D., and van Oudenaarden, A. (2013). Dampening of expression oscillations by synchronous regulation of a microRNA and its target. Nat. Genet. *45*, 1337–1344.

Kim, J., Khetarpal, I., Sen, S., and Murray, R.M. (2014). Synthetic circuit for exact adaptation and fold-change detection. Nucleic Acids Res. *42*, 6078–6089.

Korem, Y., Szekely, P., Hart, Y., Sheftel, H., Hausser, J., Mayo, A., Rothenberg, M.E., Kalisky, T., and Alon, U. (2015). Geometry of the gene expression space of individual cells. PLoS Comput. Biol. *11*, e1004224.

Larsch, J., Flavell, S.W., Liu, Q., Gordus, A., Albrecht, D.R., and Bargmann, C.I. (2015). A circuit for gradient climbing in C. elegans chemotaxis. Cell Rep. *12*, 1748–1760.

Lazova, M.D., Ahmed, T., Bellomo, D., Stocker, R., and Shimizu, T.S. (2011). Response rescaling in bacterial chemotaxis. Proc. Natl. Acad. Sci. USA *108*, 13870–13875.

Lee, R.E., Walker, S.R., Savery, K., Frank, D.A., and Gaudet, S. (2014). Fold change of nuclear NF-κB determines TNF-induced transcription in single cells. Mol. Cell *53*, 867–879.

Ma, W., Trusina, A., El-Samad, H., Lim, W.A., and Tang, C. (2009). Defining network topologies that can achieve biochemical adaptation. Cell *138*, 760–773.

Mangan, S., and Alon, U. (2003). Structure and function of the feed-forward loop network motif. Proc. Natl. Acad. Sci. USA *100*, 11980–11985.

Mangan, S., Itzkovitz, S., Zaslaver, A., and Alon, U. (2006). The incoherent feed-forward loop accelerates the response-time of the gal system of Escherichia coli. J. Mol. Biol. *356*, 1073–1081.

Marquez-Lago, T.T., and Leier, A. (2011). Stochastic adaptation and fold-change detection: from single-cell to population behavior. BMC Syst. Biol. *5*, 22.

Mesibov, R., Ordal, G.W., and Adler, J. (1973). The range of attractant concentrations for bacterial chemotaxis and the threshold and size of response over this range. Weber law and related phenomena. J. Gen. Physiol. *62*, 203–223.

Milo, R., Shen-Orr, S., Itzkovitz, S., Kashtan, N., Chklovskii, D., and Alon, U. (2002). Network motifs: simple building blocks of complex networks. Science *298*, 824–827.

Olsman, N., and Goentoro, L. (2016). Allosteric proteins as logarithmic sensors. Proc. Natl. Acad. Sci. USA *113*, E4423–E4430.

Paulsson, J. (2004). Summing up the noise in gene networks. Nature *427*, 415–418.

Raser, J.M., and O'Shea, E.K. (2005). Noise in gene expression: origins, consequences, and control. Science *309*, 2010–2013.

Rosenfeld, N., Elowitz, M.B., and Alon, U. (2002). Negative autoregulation speeds the response times of transcription networks. J. Mol. Biol. *323*, 785–793.

Savageau, M.A. (1976). Biochemical systems analysis: a study of function and design in molecular biology (Addison-Wesley: Publishing Company).

Savageau, M.A. (1988). Introduction to S-systems and the underlying power-law formalism. Math. Comput. Model. *11*, 546–551.

Savageau, M.A. (2001). Design principles for elementary gene circuits: elements, methods, and examples. Chaos *11*, 142–159.

Shah, N.A., and Sarkar, C.A. (2011). Robust network topologies for generating switch-like cellular responses. PLoS Comput. Biol. *7*, e1002085.

Shoval, O., Goentoro, L., Hart, Y., Mayo, A., Sontag, E., and Alon, U. (2010). Fold-change detection and scalar symmetry of sensory input fields. Proc. Natl. Acad. Sci. USA *107*, 15995–16000.

Shoval, O., Alon, U., and Sontag, E. (2011). Symmetry invariance for adapting biological systems. SIAM J. Appl. Dyn. Syst. *10*, 857–886.

Shoval, O., Sheftel, H., Shinar, G., Hart, Y., Ramote, O., Mayo, A., Dekel, E., Kavanagh, K., and Alon, U. (2012). Evolutionary trade-offs, Pareto optimality, and the geometry of phenotype space. Science *336*, 1157–1160.

Sigal, A., Milo, R., Cohen, A., Geva-Zatorsky, N., Klein, Y., Liron, Y., Rosenfeld, N., Danon, T., Perzov, N., and Alon, U. (2006). Variability and memory of protein levels in human cells. Nature *444*, 643–646.

Skataric, M., and Sontag, E.D. (2012a). A characterization of scale invariant responses in enzymatic networks. PLoS Comput. Biol. *8*, e1002748.

Skataric, M., and Sontag, E. (2012b). Exploring the scale invariance property in enzymatic networks. In 2012 IEEE 51st Annual Conference on Decision and Control (CDC) (IEEE), pp. 5511–5516.

Sontag, E. (2015). Incoherent feedforward motifs as immune change detectors. bioRxiv. http://dx.doi.org/10.1101/035600.

Szekely, P., Sheftel, H., Mayo, A., and Alon, U. (2013). Evolutionary tradeoffs between economy and effectiveness in biological homeostasis systems. PLoS Comput. Biol. *9*, e1003163.

Szekely, P., Korem, Y., Moran, U., Mayo, A., and Alon, U. (2015). The mass-longevity triangle: Pareto optimality and the geometry of life-history trait space. PLoS Comput. Biol. *11*, e1004524.

Takeda, K., Shao, D., Adler, M., Charest, P.G., Loomis, W.F., Levine, H., Groisman, A., Rappel, W.-J., and Firtel, R.A. (2012). Incoherent feedforward control governs adaptation of activated ras in a eukaryotic chemotaxis pathway. Sci. Signal. *5*, ra2.

Tendler, A., Mayo, A., and Alon, U. (2015). Evolutionary tradeoffs, Pareto optimality and the morphology of ammonite shells. BMC Syst. Biol. *9*, 12.

Tu, Y., Shimizu, T.S., and Berg, H.C. (2008). Modeling the chemotactic response of Escherichia coli to time-varying stimuli. Proc. Natl. Acad. Sci. USA *105*, 14855–14860.

Wang, Y., Ku, C.-J., Zhang, E.R., Artyukhin, A.B., Weiner, O.D., Wu, L.F., and Altschuler, S.J. (2013). Identifying network motifs that buffer front-to-back signaling in polarized neutrophils. Cell Rep. *3*, 1607–1616.

Warmflash, A., Francois, P., and Siggia, E.D. (2012). Pareto evolution of gene networks: an algorithm to optimize multiple fitness objectives. Phys. Biol. *9*, 056001.

Wartlick, O., Mumcu, P., Jülicher, F., and Gonzalez-Gaitan, M. (2011). Understanding morphogenetic growth control – lessons from flies. Nat. Rev. Mol. Cell Biol. *12*, 594–604.

Weber, E.H. (1905). Tastsinn und Gemeingefühl (W.: Engelmann).

Yao, G., Tan, C., West, M., Nevins, J.R., and You, L. (2011). Origin of bistability underlying mammalian cell cycle entry. Mol. Syst. Biol. *7*, 485.

Yi, T.-M., Huang, Y., Simon, M.I., and Doyle, J. (2000). Robust perfect adaptation in bacterial chemotaxis through integral feedback control. Proc. Natl. Acad. Sci. USA *97*, 4649–4653.

STAR★METHODS

KEY RESOURCES TABLE

REAGENT or RESOURCE	SOURCE	IDENTIFIER
Software and Algorithms		
NDSolveValue	mathematica10.2	N/A
Ito process	mathematica10.2	N/A
Other		
Resource website for the mathematica code	This paper	https://github.com/AlonLabWIS/FCD

CONTACT FOR REAGENT AND RESOURCE SHARING

Further information and requests for software may be directed to, and will be fulfilled by the Lead Contact Uri Alon (uri.alon@weizmann.ac.il).

METHOD DETAILS

Dimensional analysis of the S-systems dynamical equations

In order to reduce the four parameters (A, B, C, D) to a single dimensionless parameter T, we begin with our model:

$$\frac{dx}{dt} = Au^{\beta_{ux}} x^{\beta_{xx}} y^{\beta_{yx}} - Bu^{\alpha_{ux}} x^{\alpha_{xx}} y^{\alpha_{yx}} \tag{1}$$

$$\frac{dy}{dt} = Cu^{\beta_{uy}} x^{\beta_{xy}} y^{\beta_{yy}} - Du^{\alpha_{uy}} x^{\alpha_{xy}} y^{\alpha_{yy}}. \tag{2}$$

We define dimensionless parameters $\hat{x}$, $\hat{y}$, $\hat{t}$ by using the following transformation

$$x = A^{\alpha_1} B^{\alpha_2} C^{\alpha_3} D^{\alpha_4} \hat{x}$$

$$y = A^{\beta_1} B^{\beta_2} C^{\beta_3} D^{\beta_4} \hat{y}$$

$$t = A^{\gamma_1} B^{\gamma_2} C^{\gamma_3} D^{\gamma_4} \hat{t}.$$

We plug this back in Equations 1 and 2 to obtain:

$$\frac{d(A^{\alpha_1} B^{\alpha_2} C^{\alpha_3} D^{\alpha_4} \hat{x})}{d(A^{\gamma_1} B^{\gamma_2} C^{\gamma_3} D^{\gamma_4} \hat{t})} = \frac{A^{\alpha_1} B^{\alpha_2} C^{\alpha_3} D^{\alpha_4}}{A^{\gamma_1} B^{\gamma_2} C^{\gamma_3} D^{\gamma_4}} \frac{d\hat{x}}{d\hat{t}} = Au^{\beta_{ux}} (A^{\alpha_1} B^{\alpha_2} C^{\alpha_3} D^{\alpha_4} \hat{x})^{\beta_{xx}} (A^{\beta_1} B^{\beta_2} C^{\beta_3} D^{\beta_4} \hat{y})^{\beta_{yx}}$$
$$- Bu^{\alpha_{ux}} (A^{\alpha_1} B^{\alpha_2} C^{\alpha_3} D^{\alpha_4} \hat{x})^{\alpha_{xx}} (A^{\beta_1} B^{\beta_2} C^{\beta_3} D^{\beta_4} \hat{y})^{\alpha_{yx}} \tag{3}$$

$$\frac{d(A^{\beta_1} B^{\beta_2} C^{\beta_3} D^{\beta_4} \hat{y})}{d(A^{\gamma_1} B^{\gamma_2} C^{\gamma_3} D^{\gamma_4} \hat{t})} = \frac{A^{\beta_1} B^{\beta_2} C^{\beta_3} D^{\beta_4}}{A^{\gamma_1} B^{\gamma_2} C^{\gamma_3} D^{\gamma_4}} \frac{d\hat{y}}{d\hat{t}} = Cu^{\beta_{uy}} (A^{\alpha_1} B^{\alpha_2} C^{\alpha_3} D^{\alpha_4} \hat{x})^{\beta_{xy}} (A^{\beta_1} B^{\beta_2} C^{\beta_3} D^{\beta_4} \hat{y})^{\beta_{yy}}$$
$$- Du^{\alpha_{uy}} (A^{\alpha_1} B^{\alpha_2} C^{\alpha_3} D^{\alpha_4} \hat{x})^{\alpha_{xy}} (A^{\beta_1} B^{\beta_2} C^{\beta_3} D^{\beta_4} \hat{y})^{\alpha_{yy}}. \tag{4}$$

We now collect all the powers together and demand that each term in the equations will be equal to the dimensionless form, which leads to 4 equations:

$$A^{1-\alpha_1+\alpha_1\ \beta_{xx}+\beta_1\beta_{xy}+\gamma_1}\ B^{-\alpha_2+\alpha_2\beta_{xx}+\beta_2\beta_{xy}+\gamma_2}\ldots$$

$$\ldots C^{-\alpha_3+\alpha_3\ \beta_{xx}+\beta_3\ \beta_{xy}+\gamma_3}\ D^{-\alpha_4+\alpha_4\beta_{xx}+\beta_4\beta_{xy}+\gamma_4} = 1 \tag{5}$$

$$A^{\alpha_1\ \alpha_{xx}-\alpha_1+\alpha_{xy}\beta_1+\gamma_1}B^{\alpha_2\alpha_{xx}-\alpha_2+\alpha_{xy}\beta_2+\gamma_2+1}\ldots$$

$$\ldots C^{\alpha_3\alpha_{xx}-\alpha_3+\alpha_{xy}\beta_3+\gamma_3}D^{\alpha_4\alpha_{xx}-\alpha_4+\alpha_{xy}\beta_4+\gamma_4}=1 \quad (6)$$

$$A^{\alpha_1\alpha_{yx}-\alpha_1\beta_{yx}+\alpha_{yy}\beta_1-\beta_1\beta_{yy}}B^{\alpha_2\alpha_{yx}-\alpha_2\beta_{yx}+\alpha_{yy}\beta_2-\beta_2\beta_{yy}}\ldots$$

$$\ldots C^{\alpha_3\alpha_{yx}-\alpha_3\beta_{yx}+\alpha_{yy}\beta_3-\beta_3\beta_{yy}-1}\ D^{\alpha_4\alpha_{yx}-\alpha_4\beta_{yx}+\alpha_{yy}\beta_4-\beta_4\beta_{yy}+1}=1 \quad (7)$$

$$A^{\alpha_1\beta_{yx}+\beta_1\beta_{yy}-\beta_1+\gamma_1}B^{\alpha_2\beta_{yx}+\beta_2\beta_{yy}-\beta_2+\gamma_2}C^{\alpha_3\beta_{yx}+\beta_3\beta_{yy}-\beta_3+\gamma_3+1}D^{\alpha_4\beta_{yx}+\beta_4\beta_{yy}-\beta_4+\gamma_4}=T. \quad (8)$$

In the first three Equations 5, 6, and 7, each term must cancel out separately, providing 12 linear equations that we can solve to get:

$$T=A^{\frac{noma}{den}}B^{\frac{nomb}{den}}C^{\frac{nomc}{den}}D^{\frac{nomd}{den}}. \quad (9)$$

Where:

$$den=(\alpha xy-\beta xy)(\alpha yx-\beta yx)-(\alpha xx-\beta xx)(\alpha yy-\beta yy)$$

$$noma=\alpha yy(-1+\alpha xx-\beta yx)+\beta yx+\alpha xy\beta yx+\beta yy-\alpha xx\beta yy+\alpha yx(-1-\alpha xy+\beta yy)$$

$$nomb=-(1+\beta xy)\beta yx+\alpha yy(1-\beta xx+\beta yx)+\alpha yx(1+\beta xy-\beta yy)+(-1+\beta xx)\beta yy$$

$$nomc=\alpha xy(1+\alpha yx-\beta xx)+(-1+\alpha yy)\beta xx-(1+\alpha yx)\beta xy+\alpha xx(1-\alpha yy+\beta xy)$$

$$nomd=\beta xx+\beta xy+\alpha xy(-1+\beta xx-\beta yx)+\beta xy\beta yx-\beta xx\beta yy+\alpha xx(-1-\beta xy+\beta yy).$$

Definition of natural and transcriptional circuit subclasses

Natural circuits are defined by $\alpha_{xx}=1$ and $\alpha_{yy}=1$, which reduces the space of possible circuits from 3^{12} to 3^{10}. Transcriptional circuits are defined by $\alpha_{xx}=1$, $\alpha_{yy}=1$, and all the rest of the degradation rate powers equal to zero, $\alpha_{ij}=0,\ (i\neq j)$. This reduces the number of circuits to 3^6.

Analytical screen of circuit properties

A circuit is connected when u is connected to x or y: $(\alpha_{ux}\neq 0\vee\alpha_{uy}\neq 0\vee\beta_{ux}\neq 0\vee\beta_{uy}\neq 0)$ and x is connected to u or y: $(\alpha_{ux}\neq 0\vee\alpha_{yx}\neq 0\vee\alpha_{xy}\neq 0\vee\beta_{ux}\neq 0\vee\beta_{yx}\neq 0\vee\beta_{xy}\neq 0)$ and y is connected to u or x: $(\alpha_{uy}\neq 0\vee\alpha_{yx}\neq 0\vee\alpha_{xy}\neq 0\vee\beta_{uy}\neq 0\vee\beta_{yx}\neq 0\vee\beta_{xy}\neq 0)$.

The steady-state is given by

$$x_{steady\ state}=u^{\frac{(\alpha_{ux}-\beta_{ux})(\alpha_{yy}-\beta_{yy})-(\alpha_{yx}-\beta_{yx})(\alpha_{uy}-\beta_{uy})}{(\alpha_{xy}-\beta_{xy})(\alpha_{yx}-\beta_{yx})-(\alpha_{xx}-\beta_{xx})(\alpha_{yy}-\beta_{yy})}} \quad (10)$$

$$y_{steady\ state}=u^{\frac{(\alpha_{uy}-\beta_{uy})(\alpha_{xx}-\beta_{xx})-(\alpha_{xy}-\beta_{xy})(\alpha_{ux}-\beta_{ux})}{(\alpha_{xy}-\beta_{xy})(\alpha_{yx}-\beta_{yx})-(\alpha_{xx}-\beta_{xx})(\alpha_{yy}-\beta_{yy})}}. \quad (11)$$

The denominator for both equations is the same. A non-zero steady state exists unless the denominator equals 0:

$$(\alpha_{xy}-\beta_{xy})(\alpha_{yx}-\beta_{yx})=(\alpha_{xx}-\beta_{xx})(\alpha_{yy}-\beta_{yy}). \quad (12)$$

The steady state is stable when the determinant of the Jacobian at the steady state (Equations 10 and 11) is positive and its trace is negative, at least for some range of the parameters (u and T). This yields the following conditions:

$$\det J=T\,u^q\left((\alpha_{xx}-\beta_{xx})(\alpha_{yy}-\beta_{yy})-(\alpha_{xy}-\beta_{xy})(\alpha_{yx}-\beta_{yx})\right)>0 \quad (13)$$

$$trJ = u^{w}(\beta_{xx} - \alpha_{xx}) + Tu^{s}(\beta_{yy} - \alpha_{yy}) < 0. \tag{14}$$

Where q, s, and w depend only on the powers:

$$\begin{aligned} q = \frac{1}{-dj}\big(&\alpha_{ux}\alpha_{xy} - \alpha_{ux}\alpha_{yy} - \alpha_{xy}\beta_{ux} + \alpha_{yy}\beta_{ux} + \alpha_{uy}\beta_{xx} + \alpha_{ux}\alpha_{yy}\beta_{xx} - \beta_{uy}\beta_{xx} + \alpha_{yy}\beta_{uy}\beta_{xx} - \alpha_{ux}\beta_{xy} + \alpha_{ux}\alpha_{yy}\beta_{xy} + \beta_{ux}\beta_{xy} - \alpha_{yy}\beta_{ux}\beta_{xy} \\ &+ \alpha_{yx}\big(\alpha_{uy} + \alpha_{xy}\beta_{ux} + \big(-1 + \alpha_{xy}\big)\beta_{uy} - \alpha_{uy}\beta_{xx} + \beta_{uy}\beta_{xx} - \big(\alpha_{uy} + \beta_{ux}\big)\beta_{xy}\big) - \alpha_{ux}\beta_{yx} - \alpha_{ux}\alpha_{xy}\beta_{yx} + \beta_{uy}\beta_{yx} - \alpha_{xy}\beta_{uy}\beta_{yx} + \alpha_{ux}\beta_{xy}\beta_{yx} \\ &+ \alpha_{uy}\beta_{xy}\beta_{yx} - \big(\big(-1 + \alpha_{xy}\big)\big(\alpha_{ux} - \beta_{ux}\big) + \big(\alpha_{ux} + \alpha_{uy}\big)\beta_{xx}\big)\beta_{yy} + \alpha_{xx}\big(\beta_{uy} - \alpha_{yy}\big(\beta_{ux} + \beta_{uy}\big) - \beta_{uy}\beta_{yx} + \beta_{ux}\beta_{yy} + \alpha_{uy}\big(-1 + \beta_{yx}\beta_{yy}\big)\big)\big) \end{aligned}$$

$$\begin{aligned} s - w = \frac{1}{-dj}\big(&\alpha_{ux}\big(\alpha_{xy} + \alpha_{yy}\big) + \alpha_{xy}\beta_{ux} + \alpha_{yy}\beta_{ux} + \alpha_{ux}\alpha_{yy}\beta_{xx} + \beta_{uy}\beta_{xx} - \alpha_{yy}\beta_{uy}\beta_{xx} + \alpha_{ux}\beta_{xy} - \alpha_{ux}\alpha_{yy}\beta_{xy} - \beta_{ux}\beta_{xy} + \alpha_{yy}\beta_{ux}\beta_{xy} \\ &+ \alpha_{yx}\big(\alpha_{uy} + \alpha_{xy}\beta_{ux} - \big(1 + \alpha_{xy}\big)\beta_{uy} - \alpha_{uy}\beta_{xx} + \beta_{uy}\beta_{xx} + \alpha_{uy}\beta_{xy} - \beta_{ux}\beta_{xy}\big) - \alpha_{ux}\alpha_{xy}\beta_{yx} + \beta_{uy}\beta_{yx} + \alpha_{xy}\beta_{uy}\beta_{yx} + \alpha_{uy}\beta_{xy}\beta_{yx} \\ &- \alpha_{uy}\big(\beta_{xx} + \beta_{yx}\big) + \big(\big(1 + \alpha_{xy}\big)\big(\alpha_{ux}\beta_{ux}\big) + \big(-\alpha_{ux} + \alpha_{uy}\big)\beta_{xx}\big)\beta_{yy} + \alpha_{xx}\big(\alpha_{yy}\big(-\beta_{ux} + \beta_{uy}\big) + \beta_{uy}\big(-1 - \beta_{yx}\big) + \alpha_{uy}\big(1 + \beta_{yx} - \beta_{yy}\big) \\ &+ \beta_{ux}\beta_{yy}\big)\big) \end{aligned}$$

where $dj = (\alpha_{xx} - \beta_{xx})(\alpha_{yy} - \beta_{yy}) - (\alpha_{xy} - \beta_{xy})(\alpha_{yx} - \beta_{yx})$.

For FCD circuits $s - w = 0$, and therefore the stability conditions of the FCD circuits do not depend on the input signal, u.

Exact adaptation occurs when the steady state output is independent of u, and in the dimensionless equations therefore equal to 1:

$$y_{steady\ state} = u^{\frac{\left(\alpha_{uy} - \beta_{uy}\right)\left(\alpha_{xx} - \beta_{xx}\right) - \left(\alpha_{xy} - \beta_{xy}\right)\left(\alpha_{ux} - \beta_{ux}\right)}{\left(\alpha_{xy} - \beta_{xy}\right)\left(\alpha_{yx} - \beta_{yx}\right) - \left(\alpha_{xx} - \beta_{xx}\right)\left(\alpha_{yy} - \beta_{yy}\right)}} = 1. \tag{15}$$

Which leads to the following condition:

$$\left(\alpha_{uy} - \beta_{uy}\right)\left(\alpha_{xx} - \beta_{xx}\right) = \left(\alpha_{xy} - \beta_{xy}\right)\left(\alpha_{ux} - \beta_{ux}\right). \tag{16}$$

In order to avoid the trivial solution we also demand that:

$$\alpha_{xy} \neq \beta_{xy} \vee \alpha_{uy} \neq \beta_{uy} \tag{17}$$

$$\alpha_{uy} \neq \beta_{uy} \vee \alpha_{ux} \neq \beta_{ux}. \tag{18}$$

In our class of circuits the homogeneity conditions from Shoval et al. (Shoval et al., 2010) are necessary and sufficient for FCD. For FCD circuits with the symmetry of $x \sim u$, the conditions lead to:

$$\left(\alpha_{ux} + \alpha_{xx} = 1 \wedge \beta_{ux} + \beta_{xx} = 1 \wedge \alpha_{uy} + \alpha_{xy} = 0 \wedge \beta_{uy} + \beta_{xy} = 0\right). \tag{19}$$

For FCD circuits with a symmetry of $x \sim (1/u)$, the conditions yield:

$$\left(\alpha_{ux} - \alpha_{xx} = -1 \wedge \beta_{ux} - \beta_{xx} = -1 \wedge \alpha_{uy} - \alpha_{xy} = 0 \wedge \beta_{uy} - \beta_{xy} = 0\right). \tag{20}$$

Analytical solution for the Jacobian

The Jacobian of the system is given by:

$$J = \begin{pmatrix} \partial_x f(u,x,y) & \partial_y f(u,x,y) \\ \partial_x g(u,x,y) & \partial_y g(u,x,y) \end{pmatrix} = \begin{pmatrix} \beta_{xx}u^{\beta_{ux}}x^{\beta_{xx}-1}y^{\beta_{yx}} - \alpha_{xx}u^{\alpha_{ux}}x^{\alpha_{xx}-1}y^{\alpha_{yx}} & \beta_{yx}u^{\beta_{ux}}x^{\beta_{xx}}y^{\beta_{yx}-1} - \alpha_{yx}\,u^{\alpha_{ux}}x^{\alpha_{xx}}y^{\alpha_{yx}-1} \\ T\left(\beta_{xy}u^{\beta_{uy}}x^{\beta_{xy}-1}y^{\beta_{yy}} - \alpha_{xy}u^{\alpha_{uy}}x^{\alpha_{xy}-1}y^{\alpha_{yy}}\right) & T\left(\beta_{yy}u^{\beta_{uy}}x^{\beta_{xy}}y^{\beta_{yy}-1} - \alpha_{yy}u^{\alpha_{uy}}x^{\alpha_{xy}}y^{\alpha_{yy}-1}\right) \end{pmatrix}.$$

Proof that the homogeneity conditions from Shoval et al. are sufficient and necessary for FCD in the S-systems framework

We prove that for S-systems the homogeneity conditions from Shoval et al. (Shoval et al., 2010) are both sufficient and necessary for FCD given that the system has a stable steady state. The S-systems equations for three-node circuits are:

$$\frac{dx}{dt} = f(u,x,y) = u^{\beta_{ux}}x^{\beta_{xx}}y^{\beta_{yx}} - u^{\alpha_{ux}}x^{\alpha_{xx}}y^{\alpha_{yx}} \tag{21}$$

$$\frac{dy}{dt} = g(u,x,y) = T\left(u^{\beta_{uy}}x^{\beta_{xy}}y^{\beta_{yy}} - u^{\alpha_{uy}}x^{\alpha_{xy}}y^{\alpha_{yy}}\right). \tag{22}$$

The steady state of the system is derived by taking Equations 10 and 11 to zero:

$$x_{st} = u^{\frac{(\alpha xu-\beta xu)(\alpha yy-\beta yy)-(\alpha xy-\beta xy)(\alpha yu-\beta yu)}{a}} \tag{23}$$

$$y_{st} = u^{\frac{(\alpha xx-\beta xx)(\alpha yu-\beta yu)-(\alpha xu-\beta xu)(\alpha yx-\beta yx)}{a}}. \tag{24}$$

Where $a = (\alpha xy - \beta xy)(\alpha yx - \beta yx) - (\alpha xx - \beta xx)(\alpha yy - \beta yy)$.

Therefore, for the system (Equations 21 and 22) to have a steady state, the following condition must hold:

$$(\beta_{yy} - \alpha_{yy})(\beta_{xx} - \alpha_{xx}) \neq (\beta_{yx} - \alpha_{yx})(\beta_{xy} - \alpha_{xy}). \tag{25}$$

We first show that the homogeneity conditions are sufficient for FCD.

The homogeneity conditions from shoval et al. state that there exists a function $\phi(p,x)$ such that:

$$f(pu, \phi(p,x), y) = \partial_x \phi(p,x) f(u,x,y) \tag{26}$$

$$g(pu, \phi(p,x), y) = g(u,x,y) \tag{27}$$

where p is a constant scalar. Plugging in these conditions (Equations 26 and 27) in our model (Equations 21 and 22) yields the following:

$$(pu)^{\beta_{ux}} \phi(p,x)^{\beta_{xx}} y^{\beta_{yx}} - (pu)^{\alpha_{ux}} \phi(p,x)^{\alpha_{xx}} y^{\alpha_{yx}} = \partial_x \phi(p,x)\left(u^{\beta_{ux}} x^{\beta_{xx}} y^{\beta_{yx}} - u^{\alpha_{ux}} x^{\alpha_{xx}} y^{\alpha_{yx}}\right) \tag{28}$$

$$T\left((pu)^{\beta_{uy}} \phi(p,x)^{\beta_{xy}} y^{\beta_{yy}} - (pu)^{\alpha_{uy}} \phi(p,x)^{\alpha_{xy}} y^{\alpha_{yy}}\right) = T\left(u^{\beta_{uy}} x^{\beta_{xy}} y^{\beta_{yy}} - u^{\alpha_{uy}} x^{\alpha_{xy}} y^{\alpha_{yy}}\right). \tag{29}$$

By cancelling T out and rearranging Equation 29 we get:

$$y^{\beta_{yy}} u^{\beta_{uy}}\left(p^{\beta_{uy}} \phi(p,x)^{\beta_{xy}} - x^{\beta_{xy}}\right) - y^{\alpha_{yy}} u^{\alpha_{uy}}\left(p^{\alpha_{uy}} \phi(p,x)^{\alpha_{xy}} - x^{\alpha_{xy}}\right) = 0. \tag{30}$$

There are three cases in which Equation 30 holds:

Case 1: if $\beta_{yy} = \alpha_{yy}$ & $\beta_{uy} = \alpha_{uy}$ then:

$$\left(p^{\beta_{uy}}\left(\phi(p,x)^{\beta_{xy}} - \phi(p,x)^{\alpha_{xy}}\right)\right) - \left(x^{\beta_{xy}} - x^{\alpha_{xy}}\right) = 0. \tag{31}$$

Looking at the leftmost term we can see two cases:

If $(p^{\beta_{uy}}(\phi(p,x)^{\beta_{xy}} - \phi(p,x)^{\alpha_{xy}})) = F(x,p)$ is dependent of p, then each term needs to cancel out separately: $(x^{\beta_{xy}} - x^{\alpha_{xy}}) = 0$ for all x, therefore $\beta_{xy} = \alpha_{xy}$ and we get that Equation 11 becomes a trivial case of FCD: $(dy/dt) = 0$.

However, if $(p^{\beta_{uy}}(\phi(p,x)^{\beta_{xy}} - \phi(p,x)^{\alpha_{xy}})) = F(x)$ is independent of p, then p should cancel out from both terms which yields:

$$\phi(p,x) = \frac{h(x)}{p^{\frac{\beta_{uy}}{\beta_{xy}}}} = \frac{h(x)}{p^{\frac{\beta_{uy}}{\alpha_{xy}}}}, \text{ which requires again that } \beta_{xy} = \alpha_{xy}.$$

In summary, case 1 leads to a trivial case where $(dy/dt) = 0$.

Case 2: if $\beta_{yy} = \alpha_{yy}$ & $\beta_{uy} \neq \alpha_{uy}$ then y is cancelled out from Equation 30 and since Equation 30 should hold for any input function u, each term must vanish separately:

$$p^{\beta_{uy}} \phi(p,x)^{\beta_{xy}} - x^{\beta_{xy}} = 0 \tag{32}$$

$$p^{\alpha_{uy}} \phi(p,x)^{\alpha_{xy}} - x^{\alpha_{xy}} = 0. \tag{33}$$

After some algebra we get:

$$\phi(p,x) = p^{-\frac{\beta_{uy}}{\beta_{xy}}} x \tag{34}$$

$$\phi(p,x) = p^{-\frac{\alpha_{uy}}{\alpha_{xy}}} x. \tag{35}$$

Therefore, we get that $\phi(p,x)=p^{\omega}x$, with $\omega=-(\beta_{uy}/\beta_{xy})=-(\alpha_{uy}/\alpha_{xy})$.
If $\beta_{xy}=0$ or $\alpha_{xy}=0$, then only Equation 35 or 34 holds respectively.
If both $\beta_{xy},\ \alpha_{xy}$ equal to 0, the dependence of x vanishes and the dependence in p cannot be scaled out.
Now we shall plug this (Equations 34 and 35) into Equation 28 which yields:

$$u^{\beta_{ux}}x^{\beta_{xx}}y^{\beta_{yx}}\left(p^{\omega\beta_{xx}+\beta_{ux}}-p^{\omega}\right)=u^{\alpha_{ux}}x^{\alpha_{xx}}y^{\alpha_{yx}}\left(p^{\omega\alpha_{xx}+\alpha_{ux}}-p^{\omega}\right). \tag{36}$$

For Equation 25 to hold, we need each term to cancel out separately. Thus we get:

$$\omega=\frac{\beta_{ux}}{1-\beta_{xx}}=\frac{\alpha_{ux}}{1-\alpha_{xx}}. \tag{37}$$

Case 3: $\beta_{yy}\neq\alpha_{yy}$ & $p^{\beta_{uy}}\phi(p,x)^{\beta_{xy}}-x^{\beta_{xy}}\neq 0$ & $p^{\alpha_{uy}}\phi(p,x)^{\alpha_{xy}}-x^{\alpha_{xy}}\neq 0$.
Therefore, we can solve Equation 30 for y:

$$y=\left(u^{\beta yu-\alpha yu}\frac{\left(x^{\beta yx}-p^{\beta yu}\phi(p,x)^{\beta yx}\right)}{\left(x^{\alpha yx}-p^{\alpha yu}\phi(p,x)^{\alpha yx}\right)}\right)^{\frac{1}{\alpha yy-\beta yy}}. \tag{38}$$

Solving Equations 26 and 27 at steady state yields the new steady state:

$$\phi_{st}=p^{\frac{(\alpha xu-\beta xu)(\alpha yy-\beta yy)-(\alpha xy-\beta xy)(\alpha yu-\beta yu)}{a}}x_{st}. \tag{39}$$

Plugging in the steady state for $x,\ y,\phi$ in Equation 38 results in the equivalent condition for $y_{st}=1$:

$$(\alpha xx-\beta xx)(\alpha yu-\beta yu)-(\alpha xu-\beta xu)(\alpha yx-\beta yx)=0. \tag{40}$$

Plugging in the expression for y (Equation 38) in Equation 30 yields:

$$u^{\alpha xu+\frac{\alpha xy(-\alpha yu+\beta yu)}{\alpha yy-\beta yy}}\left(\frac{x^{\beta yx}-p^{\beta yu}\phi(p,x)^{\beta yx}}{x^{\alpha yx}-p^{\alpha yu}\phi(p,x)^{\alpha yx}}\right)^{\frac{\alpha xy-\beta xy}{\alpha yy-\beta yy}}\left(p^{\alpha xu}\phi(p,x)^{\alpha xx}-x^{\alpha xx}\partial_x\phi(p,x)\right)=u^{\beta xu+\frac{\beta xy(-\alpha yu+\beta yu)}{\alpha yy-\beta yy}}\left(p^{\beta xu}\phi(p,x)^{\beta xx}-x^{\beta xx}\partial_x\phi(p,x)\right). \tag{41}$$

The powers of u in Equation 41 cannot be cancelled out in order to obey the conditions for the existence of the steady state and its solution (Equations 25 and 40). Therefore, only if both terms will vanish separately Equation 41 holds. Solving this yields back to case 2.

Therefore, under the homogeneity conditions the model (Equations 21-22) can be written in the following way (from Equations 34, 35, 37):

$$\frac{dx}{dt}=u^{\omega}\left(\left(\frac{x}{u^{\omega}}\right)^{\beta_{xx}}y^{\beta_{yx}}-\left(\frac{x}{u^{\omega}}\right)^{\alpha_{xx}}y^{\alpha_{yx}}\right) \tag{42}$$

$$\frac{dy}{dt}=T\left(\left(\frac{x}{u^{\omega}}\right)^{\beta_{xy}}y^{\beta_{yy}}-\left(\frac{x}{u^{\omega}}\right)^{\alpha_{xy}}y^{\alpha_{yy}}\right). \tag{43}$$

Let us see that the dynamics is indeed FCD: for that we need to show that under the scaling $u\to p\,u,\ x\to\tilde{x}$, the output stays the same: $y\to y$. Taking $u\to p\,u$, Equations 42 and 43 yields:

$$\frac{dx}{dt}=(pu)^{\omega}\left(\left(\frac{x}{(pu)^{\omega}}\right)^{\beta_{xx}}y^{\beta_{yx}}-\left(\frac{x}{(pu)^{\omega}}\right)^{\alpha_{xx}}y^{\alpha_{yx}}\right) \tag{44}$$

$$\frac{dy}{dt}=T\left(\left(\frac{x}{(pu)^{\omega}}\right)^{\beta_{xy}}y^{\beta_{yy}}-\left(\frac{x}{(pu)^{\omega}}\right)^{\alpha_{xy}}y^{\alpha_{yy}}\right). \tag{45}$$

If we consider that $\tilde{x}\to(x/p^{\omega})$ we get the same equations but with a different variable:

$$\frac{d\tilde{x}}{dt}=u^{\omega}\left(\left(\frac{\tilde{x}}{u^{\omega}}\right)^{\beta_{xx}}y^{\beta_{yx}}-\left(\frac{\tilde{x}}{u^{\omega}}\right)^{\alpha_{xx}}y^{\alpha_{yx}}\right) \tag{46}$$

$$\frac{dy}{dt}=T\left(\left(\frac{\tilde{x}}{u^{\omega}}\right)^{\beta_{xy}}y^{\beta_{yy}}-\left(\frac{\tilde{x}}{u^{\omega}}\right)^{\alpha_{xy}}y^{\alpha_{yy}}\right). \tag{47}$$

The dynamics will remain the same and we will end up with the same output, therefore FCD holds.

We now show that the homogeneity conditions from Shoval et al. are also necessary for FCD.

Let us assume that the model (Equations 21 and 22) shows FCD:

We first assume that there is exact adaptation. In our model this means that the steady state of the output (Equation 24) does not depend on u, this leads to a demand on the powers:

$$(\alpha xx - \beta xx)(\alpha yu - \beta yu) - (\alpha xu - \beta xu)(\alpha yx - \beta yx) = 0 \tag{48}$$

$$\beta yx = \frac{\alpha yx(\alpha xu - \beta xu) - (\alpha xx - \beta xx)(\alpha yu - \beta yu)}{\alpha xu - \beta xu}. \tag{49}$$

We can plug this into Equation 23 and get a simpler steady state term for x:

$$x_{st} = u^{\frac{\beta xu - \alpha xu}{\alpha xx - \beta xx}} \equiv u^{\delta}. \tag{50}$$

FCD means that by multiplying the input by a constant scale factor p: $u \to pu$, we get the same dynamics of the output where the internal variable can also scale somehow, $x \to \tilde{x}$.

$$\frac{d\tilde{x}}{dt} = (pu)^{\beta_{ux}} \tilde{x}^{\beta_{xx}} y^{\beta_{yx}} - (pu)^{\alpha_{ux}} \tilde{x}^{\alpha_{xx}} y^{\alpha_{yx}} \tag{51}$$

$$\frac{dy}{dt} = T\left((pu)^{\beta_{uy}} \tilde{x}^{\beta_{xy}} y^{\beta_{yy}} - (pu)^{\alpha_{uy}} \tilde{x}^{\alpha_{xy}} y^{\alpha_{yy}}\right). \tag{52}$$

Let us assume that the system is at steady state with some $u = u_0$ and suddenly, at $t = 0$, the input value changes in step-like manner to u_f. At this instance the system will respond in the following manner:

$$\left.\frac{d\tilde{x}}{dt}\right|_{t=0} = u_f^{\beta_{ux}} u_0^{\delta\beta_{xx}} - u_f^{\alpha_{ux}} u_0^{\delta\alpha_{xx}} \tag{53}$$

$$\left.\frac{dy}{dt}\right|_{t=0} = T\left(u_f^{\beta_{uy}} u_0^{\delta\beta_{xy}} - u_f^{\alpha_{uy}} u_0^{\delta\alpha_{xy}}\right). \tag{54}$$

Since it is an FCD system, the output stays the same if both u_0 and u_f are multiplied by P

$$T\left(u_f^{\beta_{uy}} u_0^{\delta\beta_{xy}} - u_f^{\alpha_{uy}} u_0^{\delta\alpha_{xy}}\right) = T\left((p\,u_f)^{\beta_{uy}} (p\,u_0)^{\delta\beta_{xy}} - (p\,u_f)^{\alpha_{uy}} (p\,u_0)^{\delta\alpha_{xy}}\right). \tag{55}$$

This must hold for every u_0 and u_f we choose, so we end up with the following constraint:

$$\alpha_{uy} + \delta\alpha_{xy} = \beta_{uy} + \delta\beta_{xy} = 0. \tag{56}$$

By changing the variables $x \to u_0^{\delta}(1 + (\Delta x/u_0^{\delta}))$, $\tilde{x} \to p^{\delta} u_0^{\delta}(1 + (\Delta\tilde{x}/p^{\delta}u_0^{\delta}))$ and plugging this into Equations 23 and 42 we get:

$$\frac{dy}{dt} = T\left(u^{-\delta\,\beta_{xy}} \left(u_0^{\delta}\left(1 + \frac{\Delta x}{u_0^{\delta}}\right)\right)^{\beta_{xy}} y^{\beta_{yy}} - u^{-\delta\alpha_{xy}} \left(u_0^{\delta}\left(1 + \frac{\Delta x}{u_0^{\delta}}\right)\right)^{\alpha_{xy}} y^{\alpha_{yy}}\right) \tag{57}$$

$$\frac{dy}{dt} = T\left(p^{-\delta\beta_{xy}} u^{-\delta\,\beta_{xy}} \left(p^{\delta} u_0^{\delta}\left(1 + \frac{\Delta\tilde{x}}{p^{\delta}u_0^{\delta}}\right)\right)^{\beta_{xy}} y^{\beta_{yy}} - p^{-\delta\alpha_{xy}} u^{-\delta\alpha_{xy}} \left(p^{\delta} u_0^{\delta}\left(1 + \frac{\Delta\tilde{x}}{p^{\delta}u_0^{\delta}}\right)\right)^{\alpha_{xy}} y^{\alpha_{yy}}\right) \tag{58}$$

We use $(1+A)^B = \Sigma_{k=0}^{\infty}\binom{B}{k}A^k$, where $\binom{B}{k}$ is the generalization of the 'choose' operator to include real numbers using Γ functions instead of regular factorial.

For a given magnitude of Δx we can truncate the series at a different value of k to get approximations for the dynamics. Therefore, each term of the sum must be equal separately.

$$\begin{aligned} T\left(u^{-\delta\,\beta_{xy}}\, u_0^{\delta\,\beta_{xy}} \binom{\beta_{xy}}{k} \left(\frac{\Delta x}{u_0^{\delta}}\right)^k y^{\beta_{yy}} - u^{-\delta\alpha_{xy}} u_0^{\delta\alpha_{xy}} \binom{\alpha_{xy}}{k} \left(\frac{\Delta x}{u_0^{\delta}}\right)^k y^{\alpha_{yy}}\right) = T\Bigg(p^{-\delta\beta_{xy}} u^{-\delta\,\beta_{xy}} p^{\delta\,\beta_{xy}} u_0^{\delta\,\beta_{xy}} \binom{\beta_{xy}}{k} \left(\frac{\Delta\tilde{x}}{p^{\delta}u_0^{\delta}}\right)^k y^{\beta_{yy}} \\ - p^{-\delta\alpha_{xy}} u^{-\delta\alpha_{xy}} p^{\delta\,\alpha_{xy}} u_0^{\delta\,\alpha_{xy}} \binom{\alpha_{xy}}{k} \left(\frac{\Delta\tilde{x}}{p^{\delta}u_0^{\delta}}\right)^k y^{\alpha_{yy}}\Bigg). \end{aligned} \tag{59}$$

Which can be further simplified:

$$\left(\left(\frac{\Delta\tilde{x}}{p^{\delta}}\right)^{k}-(\Delta x)^{k}\right)\left(u^{-\delta\alpha_{xy}}u_0^{\delta\,\alpha_{xy}}\binom{\alpha_{xy}}{k}y^{\alpha_{yy}}-u^{-\delta\,\beta_{xy}}\,u_0^{\delta\,\beta_{xy}}\binom{\beta_{xy}}{k}\,y^{\beta_{yy}}\right)=0. \tag{60}$$

We have two cases:

Case 1:

$$\left(u^{-\delta\alpha_{xy}}u_0^{\delta\,\alpha_{xy}}\binom{\alpha_{xy}}{k}y^{\alpha_{yy}}-u^{-\delta\,\beta_{xy}}\,u_0^{\delta\,\beta_{xy}}\binom{\beta_{xy}}{k}\,y^{\beta_{yy}}\right)=0. \tag{61}$$

This is a special fine-tuned, k dependent argument. If this was to cancel out for every k, we need u, u_0, or y to be 0, which is problematic for FCD systems.

Case 2:

$$\left(\frac{\Delta\tilde{x}}{p^{\delta}}\right)^{k}-(\Delta x)^{k}=0\Rightarrow\quad\Delta\tilde{x}=p^{\delta}\,\Delta x \tag{62}$$

$$\tilde{x}=p^{\delta}u_0^{\delta}\left(1+\frac{\Delta\tilde{x}}{p^{\delta}u_0^{\delta}}\right)=\;p^{\delta}u_0^{\delta}\left(1+\frac{p^{\delta}\,\Delta x}{p^{\delta}u_0^{\delta}}\right)=\;p^{\delta}u_0^{\delta}\left(1+\frac{\Delta x}{u_0^{\delta}}\right)=p^{\delta}x. \tag{63}$$

Now we can plug this into Equations 51 and 52:

$$\frac{dp^{\delta}x}{dt}=(pu)^{\beta_{ux}}\left(p^{\delta}x\right)^{\beta_{xx}}y^{\beta_{yx}}-(pu)^{\alpha_{ux}}\left(p^{\delta}x\right)^{\alpha_{xx}}y^{\alpha_{yx}} \tag{64}$$

$$\frac{dy}{dt}=T\left((pu)^{\beta_{uy}}\left(p^{\delta}x\right)^{\beta_{xy}}y^{\beta_{yy}}-(pu)^{\alpha_{uy}}\left(p^{\delta}x\right)^{\alpha_{xy}}y^{\alpha_{yy}}\right). \tag{65}$$

From Equation 64 we get:

$$p^{-\delta}(pu)^{\beta_{ux}}\left(p^{\delta}x\right)^{\beta_{xx}}y^{\beta_{yx}}-p^{-\delta}(pu)^{\alpha_{ux}}\left(p^{\delta}x\right)^{\alpha_{xx}}y^{\alpha_{yx}}=\;u^{\beta_{ux}}x^{\beta_{xx}}y^{\beta_{yx}}-u^{\alpha_{ux}}x^{\alpha_{xx}}y^{\alpha_{yx}} \tag{66}$$

$$\left(p^{-\delta+\beta_{ux}+\delta\beta_{xx}}-1\right)\;u^{\beta_{ux}}x^{\beta_{xx}}y^{\beta_{yx}}=\left(p^{-\delta+\alpha_{ux}+\delta\alpha_{xx}}-1\right)u^{\alpha_{uy}}x^{\alpha_{xy}}y^{\alpha_{yy}}. \tag{67}$$

This must hold for all p, therefore:

$$-\delta+\beta_{ux}+\delta\beta_{xx}=\;-\delta+\alpha_{ux}+\delta\alpha_{xx}=0. \tag{68}$$

Given $\delta=(\beta xu-\alpha xu)/(\alpha xx-\beta xx)$ we get:

$$\delta=\frac{\beta xu}{\beta xx-1}=\frac{\alpha xu}{\alpha xx-1}. \tag{69}$$

Equation 69 is exactly what we got from the homogeneity conditions.

The FCD circuits in our screen show a symmetry

Given the conditions on the powers (Equation 16) for FCD, our model can be written in the following way:

$$\frac{dx}{dt}=u\left(\left(\frac{x}{u}\right)^{\beta_{xx}}y^{\beta_{yx}}-\left(\frac{x}{u}\right)^{\alpha_{xx}}y^{\alpha_{yx}}\right) \tag{70}$$

$$\frac{dy}{dt}=T\left(\left(\frac{x}{u}\right)^{\beta_{xy}}y^{\beta_{yy}}-\left(\frac{x}{u}\right)^{\alpha_{xy}}y^{\alpha_{yy}}\right). \tag{71}$$

In this class of FCD circuits $x\sim u$.

Given the conditions on the powers (Equation 20) for the class of FCD circuits in which $x\sim 1/u$, the model can be written in the following way:

$$\frac{dx}{dt}=\frac{1}{u}\left((ux)^{\beta_{xx}}y^{\beta_{yx}}-(ux)^{\alpha_{xx}}y^{\alpha_{yx}}\right) \tag{72}$$

$$\frac{dy}{dt} = T\left((ux)^{\beta_{xy}} y^{\beta_{yy}} - (ux)^{\alpha_{xy}} y^{\alpha_{yy}}\right). \quad (73)$$

Taking $u \to 1/u$ in Equations 70 and 71 yields Equations 72 and 73 hence the symmetry.

Speed and amplitude calculation

We evaluated the amplitude and response time as defined in the Results section for each circuit using numerical integration with the NDSolveValue function of mathematica10.2. We tested various input step fold-changes, and found that the same circuits are on the Pareto front for steps larger than 21-fold. For steps smaller than 21, the observed circuits are still on the Pareto front, and a small number of additional circuits join the front as well (see Figure S4 for step input u = 2).

Noise resistance calculation

For the noise resistance calculation we used an Ito process (ItoProcess function of mathematica10.2) with the following form:

$$dx = f(u,x,y)dt + \frac{1}{2}x\, d\omega_1 \quad (74)$$

$$dy = g(u,x,y)dt + \frac{1}{2}y\, d\omega_2. \quad (75)$$

The ω's are stochastic Gaussian noise variables (Weiner process) determined at time steps of 0.1 in the interval between 0 and 10 time units. We repeated this simulation 50 times and took the median deviation from the steady state of y.

FCD circuits in which the internal node x is faster than the output y (T = 0.1)

The main text described the cases of T = 1 and T = 10. There is another case in which x is faster than y, where the dimensionless timescale ratio, T, is small (e.g., T = 0.1). To our knowledge, FCD hasn't been shown experimentally in this regime; I1FFL systems with micro-RNAs playing the role of x could be possible candidates (Ebert and Sharp, 2012; Kim et al., 2013). We repeated the computation of the four tasks: speed, response amplitude, economy and noise resistance for FCD circuits with T = 0.1 (Figures S1 and S3).

Cell Systems, Volume *4*

Supplemental Information

Optimal Regulatory Circuit Topologies for Fold-Change Detection

Miri Adler, Pablo Szekely, Avi Mayo, and Uri Alon

Supplemental Figures

Figure S1, related to Figure 3.

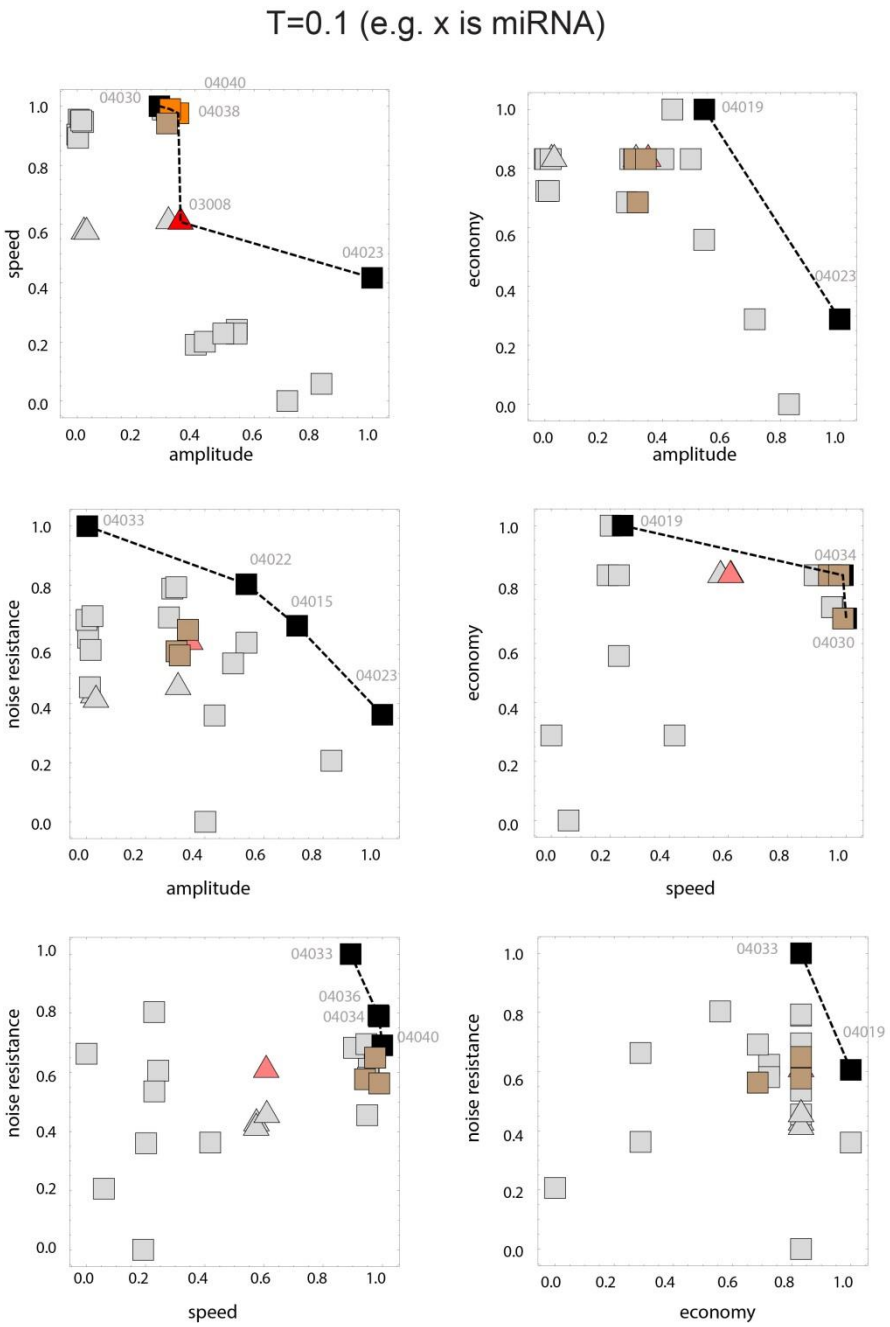

Figure S1. The I1FFL circuit is on the Pareto front for amplitude versus speed for T=0.1. Similar to figure 3 in the main text only with T=0.1.

Figure S2, related to Figure 5.

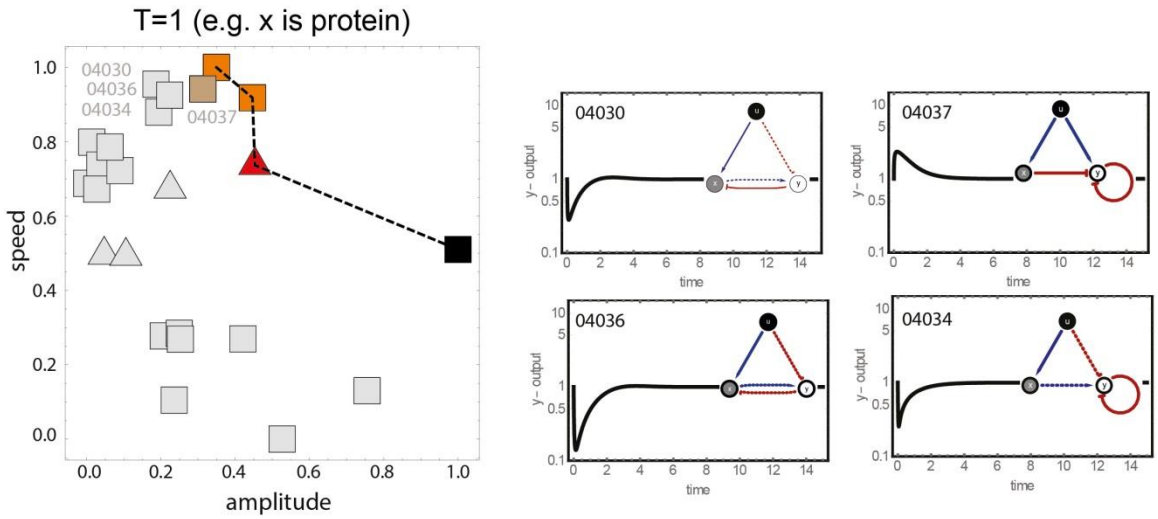

Figure S2. Dynamics of circuits that lie close to the Pareto front. Similar to figure 5a in the main text with topology and dynamics of the circuits that lie close to the front.

Figure S3, related to Figure 5.

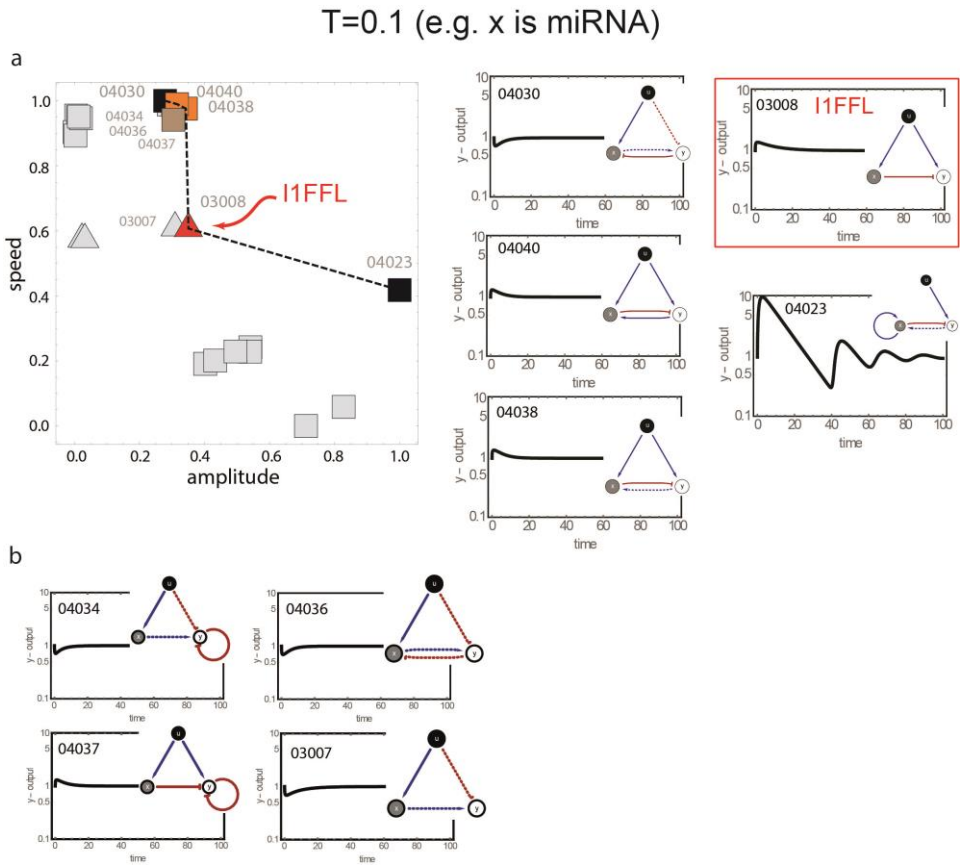

Figure S3. The speed-amplitude Pareto front suggests several FCD circuits with optimal tradeoff. (a) Similar to figure 5 in the main text with T=0.1. (b) Topology and dynamics of the circuits that lie close to the Pareto front for T=0.1.

Figure S4, related to Figure 5.

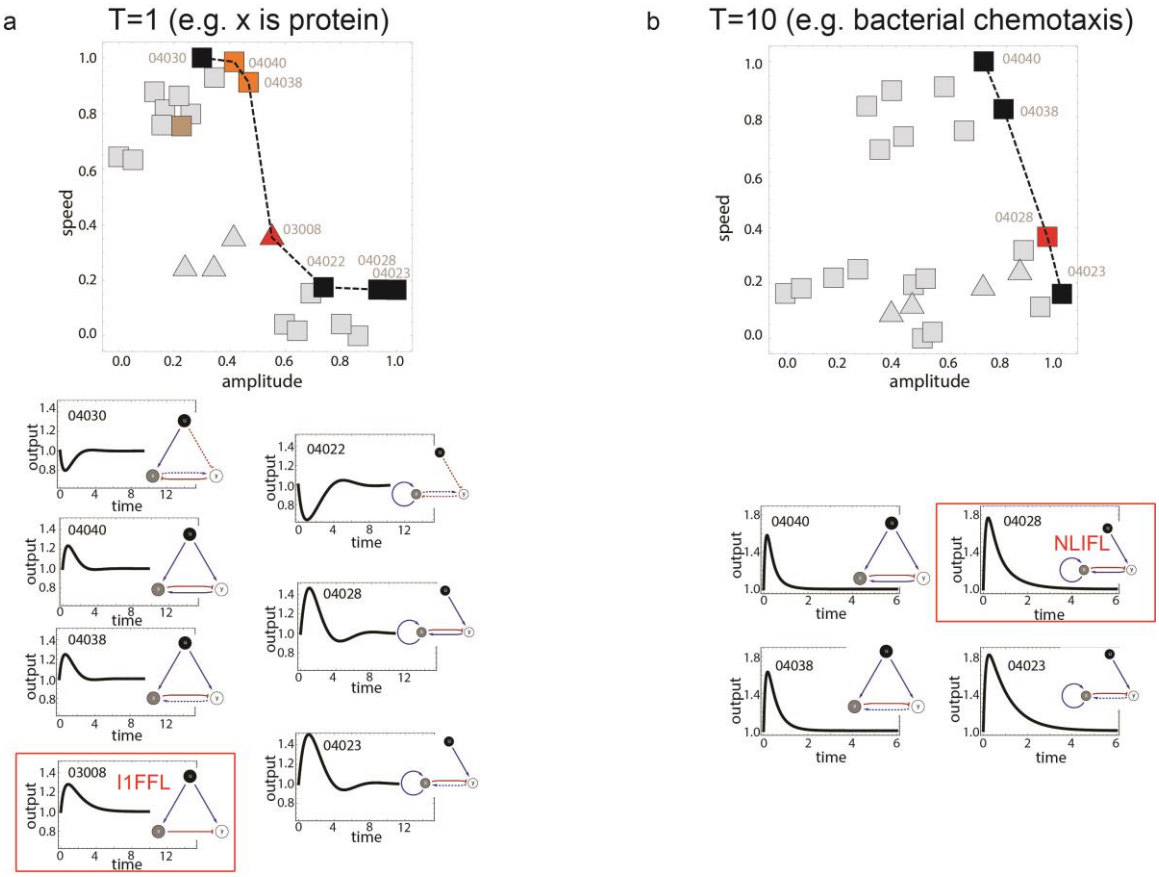

Figure S4. The experimentally observed circuits are on the Pareto front for speed and amplitude. Similar to figure 5 in the main text only with a fold step of 2 in the input.

Table S1, related to Figure 3. List of all FCD circuit topologies, their dynamical equations, and their values for the four tasks for T=0.1, 1 and 10. Missing values indicate tasks which could not be computed due to numerical problems, mostly in the presence of noise; Of the 74 FCD circuits considered in the main text (natural FCD circuits with up to 5 interactions), 6 have missing values in noise resistance.